Title	Formation of an ultracarbonaceous Antarctic micrometeorite through minimal aqueous alteration in a small porous icy body
Author(s)	Yabuta, Hikaru; Noguchi, Takaaki; Itoh, Shoichi; Nakamura, Tomoki; Miyake, Akira; Shinichi, Tsujimoto; Ohashi, Noriaki; Sakamoto, Naoya; Hashiguchi, Minako; Abe, Ken-ichi; Okubo, Aya; Kilcoyne, A. L. David; Tachibana, Shogo; Okazaki, Ryuji; Terada, Kentaro; Ebihara, Mitsuru; Nagahara, Hiroko
Citation	Geochimica et Cosmochimica Acta , 214 : 172 - 190
Issue Date	2017-10-01
DOI	10.1016/j.gca.2017.06.047
Self DOI	
URL	https://ir.lib.hiroshima-u.ac.jp/00048703
Right	© 2017. This manuscript version is made available under the CC-BY-NC-ND 4.0 license http://creativecommons.org/licenses/by-nc-nd/4.0/ This is not the published version. Please cite only the published version. この論文は出版社版でありません。引用の際には出版社版をご確認、ご利用ください。
Relation	

Formation of an Ultracarbonaceous Antarctic Micrometeorite through Minimum Aqueous Alteration in a Small Porous Icy Body

Hikaru Yabuta[1 †] , Takaaki Noguchi[2], Shoichi Itoh[3], Tomoki Nakamura[4], Akira Miyake[3], Shinichi Tsujimoto[5], Noriaki Ohashi[5], Naoya Sakamoto[6], Minako Hashiguchi[7], Ken-ichi Abe[6], Aya Okubo[8], A. L. David Kilcoyne[9], Shogo Tachibana[6], Ryuji Okazaki[7], Kentaro Terada[10], Mitsuru Ebihara[11] and Hiroko Nagahara[8]

[1] Department of Earth and Planetary Systems Science, Hiroshima University, 1-3-1 Kagamiyama, Hiroshima 739-8526, Japan

[2] Faculty of Arts and Science, Kyushu University, 744 Motooka, Nishi-ku, Fukuoka 819-0395, Japan

[3] Faculty of Science, Kyoto University, Kitashirakawa Oiwake-cho, Sakyo-ku, Kyoto 606-8502, Japan

[4] Department of Earth Science, Tohoku University, 6-3 Aramaki Aza Aoba, Aoba, Sendai,

Miyagi 980-8578, Japan

[5] College of Science, Ibaraki University, 2-1-1, Bunkyo, Mito, 310-8512, Japan

[6] Department of Natural History Sciences, Hokkaido University, N10W8, Kita-ku, Sapporo 060-0810, Japan

[7] Faculty of Science, Kyushu University, 744 Motooka, Nishi-ku, Fukuoka 819-0395, Japan

[8] Department of Earth and Planetary Science, The University of Tokyo, 7-3-1 Hongo, Bunkyo-ku, Tokyo 113-0033 Japan

[9] Advanced Light Source, Lawrence Berkeley National Laboratory, 6 Cyclotron Rd., Berkeley, CA 94720, USA

[10] Department of Earth and Space Science, Osaka University, 1-1 Machikaneyama, Toyonaka, Osaka 560-0043, Japan

[11] Department of Chemistry, Tokyo Metropolitan University, 1-1 Minami-Osawa, Hachioji, Tokyo 192-0397, Japan

[†] Corresponding author: Tel: +81-82-424-7474; Fax: +81-82-424-0735

E-mail address: hyabuta@hiroshima-u.ac.jp

Keywords: Ultracarbonaceous Antarctic micrometeorites, organic matter, GEMS, aqueous alteration, comet, shock, SIMS, XANES, TEM

Abstract

A comprehensive study of organic chemistry and mineralogy of an ultracarbonaceous micrometeorite (UCAMM D05IB80), collected from near the Dome Fuji Station, Antarctica, has been carried out in order to understand the genetic relationship among organic materials, silicates, and water. The micrometeorite is composed of a dense aggregate of ~5-μm-sized hollow ellipsoidal organic material containing submicrometer-sized phases such as GEMS and mineral grains. There is a wide area of organic material (~15 x 15 μm) in its interior. Low-Ca pyroxene is much more abundant than olivine and shows various Mg/(Mg+Fe) ratios from ~1.0 to 0.78, which is common to previous works of UCAMM. By contrast, GEMS grains in this UCAMM have unusual chemical compositions. They are depleted in both Mg and S, which suggests that these elements were leached out from the GEMS grains during very weak aqueous alteration without forming phyllosilicates.

The organics show two types of texture, smooth and globular with an irregular outline, and both of them are composed of imine, nitrile and/or aromatic nitrogen heterocycles, and

amide. The ratio of nitrogen to carbon (N/C) in the smooth region of the organics is ~0.15, which is five times higher than insoluble organic macromolecules in types 1 and 2 chondritic meteorites. In addition, the UCAMM organics is soluble in epoxy, and thus it has hydrophilicity. These polar natures indicate that the organic material in the UCAMM is very primitive. The surface of the organics is coated with an inorganic layer with a few nanometers thickness, which consists of C, O, Si, S, and Fe. Sulfur is also contained in the interior, implying the presence of organosulfur moieties. There is no isotopic anomaly of D, ^{13}C and ^{15}N in the organic material.

Since interstellar photochemistry alone would not be able to explain the N/C ratio of the UCAMM organics, we suggest that very small amount of fluid on a comet must have been necessary for the formation of UCAMM. The GEMS grains depleted in Mg and S in the UCAMM prove a very weak degree of aqueous alteration, which is weaker than that of carbonaceous chondrites. Short-duration weak alteration probably caused by planetesimal shock locally melts cometary ice grains and releases water that dissolves organics, while the fluid unlikely mobilizes because of very low thermal conductivity of the porous icy body. This event allows formation of a large organic puddle of the UCAMM, as well as organic matter sulfurization, formation of mineral membrane-like thin layers, and deformation of organic nanoglobules.

(408 words (max. 500 words))

1. Introduction

Interstellar dusts that accreted to form a protoplanetary disk are thought to be micron-sized particles consisting of an amorphous silicate core, a refractory organic mantle, and an outer mantle of ice (Greenberg and Li, 1997). Because of the large difference in the thermal stability of these three components, the grains are expected to change their composition according to thermal processing in a protoplanetary disk. The association of reactive components, amorphous silicates, organic materials, and water, in a single grain suggests possible interactions among the three components. It has been recently well recognized that organic materials in chondrites were the aqueously and/or thermally processed products in parent bodies and that their chemical and isotopic signatures were modified (e.g., Alexander et al., 2007). It is, however, not known what the precursor materials were and under what the conditions organics were processed in chondrite parent bodies. Therefore, it is important to trace back to the evolution and interactions among silicates and organic materials, and ice in the proto-solar disk and their consequence in parent bodies. It requires us to study organics as primitive as possible, which might correspond to the materials other than those found in chondrites.

Interplanetary dust particles (IDPs) and Antarctic micrometeorites (AMMs) are one of the most primitive Solar System materials available to us and one of the most suitable objects for an *in-situ* study on the origin of and spatial relationship between organic and inorganic materials formed in the early Solar System. Chondritic porous (CP)-IDPs are thought to have a link with short period comets (Messenger et al. 2006), based on their fine-grained, porous, and fragile structure (Bradley and Brownlee, 1986), high abundance of carbon (~12%, Thomas et al. 1994), and the presence of sub-micron silicate glass with embedded metal and sulfides (GEMS) (Bradley et al. 1999). It has been also known that D- and ^{15}N- enrichments of the organics in CP-IDPs (e.g., Messenger, 2000; Floss et al. 2004) and IDPs from the comet 26P/Grigg–Skjellerup dust stream (Busemann et al. 2009) resemble those found in the primitive types 1 and 2 carbonaceous chondrites (Busemann et al., 2006; Nakamura-Messenger et al. 2006). Recently, AMMs containing porous aggregates of GEMS and enstatite whisker/platelets, which are similar morphology and mineralogy to CP-IDPs, have been identified (Noguchi et al. 2015). Both IDPs and AMMs are thus the key extraterrestrial materials to enhance our understanding of the relationship between comets and meteorites.

Of the AMMs, ultracarbonaceous micrometeorites (UCAMMs) are unique extraterrestrial materials that contain a large amount of carbonaceous materials. They were collected for the first time by the 46th and 47th Japan Antarctic Research Expedition (JARE) teams from the virgin surface snow near the Dome Fuji Station, Antarctica, and reported to have pristine nature in terms of mineralogy and chemistry (Nakamura et al. 2005). One of the UCAMMs contains light noble gases with solar wind origin, and two contain high abundance of presolar grains (Yada et al. 2008; Floss et al. 2012). UCAMMs have been independently found in Antarctica by the French-Italian team, which are characterized by D-enrichment in organic matter (Duprat et al. 2010). The degree of D-enrichment is by factors to an order of magnitude larger than the terrestrial value. Duprat et al. (2010) has discussed that organic materials in UCAMMs could be produced in the outer protoplanetary disk, based on the identification of crystalline minerals that are thought to be solar origin and are embedded in the organic material. Dartois et al. (2013) have further reported ^{15}N- and D-rich micrometeorites and have proposed that the nitrogen-rich organic material in UCAMM was formed by irradiation of CH_4 - and N_2 -rich ice in the Oort cloud.

In the present study, we have made a comprehensive mineralogical and organic chemical study of a UCAMM and suggest a new pathway for the formation of UCAMMs through the interaction of organics, silicates, and water in the very early stage of alteration in a parent body.

2. Experimental

The Antarctic snow, collected by the 51st JARE team of the National Institute of Polar Research (NIPR), was melted and filtered in a class 1000 clean room at Ibaraki University, and the residual particles were manually picked up under a binocular microscope. Details of the micrometeorite collecting method are described by Sakamoto et al. (2010). They were observed with JEOL JSM-5600LV scanning electron microscope (SEM) equipped with energy dispersive spectrometer (EDS) at Ibaraki University and micrometeorites were selected from terrestrial materials based on the morphology and EDS spectra with chondritic composition rich in Si, Mg, Fe, and O (see electronic supplementary data, S1). About 90 micrometeorites were identified from fine-grained particles collected from ~100 kg of the snow. When the intensity of C kα peak exceeds twice that of O kα, it was classified as an UCAMM in this study, and only one, D05IB80, was identified as an UCAMM. Bulk mineralogy of D05IB80 was investigated by using synchrotron radiation X-ray diffraction (SR-XRD) at the Photon Factory Institute of Materials Structure Science, High Energy Accelerator Research Organization, Tsukuba, Japan.

Raman spectroscopy of the UCAMM D05IB80 was performed by JASCO NRS-3100

Raman spectrometer equipped with the 785-nm excitation laser at Ibaraki University. The beam diameter of the laser was ~ 2 μm, and the laser power was suppressed below 1 mW to avoid decomposition of carbonaceous material.

Next, UCAMM D05IB80 was embedded in epoxy resin and ultramicrotomed into 70-nm-thick sections. After ultramicrotomy, the potted butt of the micrometeorite was embedded again in epoxy resin and the surface was polished to make a flat epoxy disk (6 mm in diameter) for the isotopic mapping analysis with a SIMS at the Hokkaido University (Cameca ims-1270 SIMS equipped with SCAPS) (Yurimoto et al. 2003). Schematic diagrams to show the 3D relationships among the ultrathin samples (ultramicrotomed sections and a FIB section) and the flat sample of this UCAMM is presented in Fig. A1.

A ~100 - ~200 pA Cs^+ primary beam in the aperture illumination mode of SIMS was used to achieve uniform secondary ion emission from a sample area of ~ 30 × 40 μm^2. A normal incident electron gun was used to compensate for sample charging and the exit slit was narrow enough to eliminate the contribution of interference ions to the isotope images. Isotopographs of $^{16}O^-$, $^{12}C^{14}N^-$, $^{32}S^-$, $^{1}H^-$, $^{2}D^-$, $^{1}H^-$, $^{16}O^-$, $^{12}C^{14}N^-$ and $^{32}S^-$ were acquired in this order, where a 150-μm contrast aperture (CA) was applied for H and D isotopographs and a 50-μm CA for $^{16}O^-$, $^{12}C^{14}N^-$ and $^{32}S^-$ isotopographs in order to obtain high lateral spatial resolution. The exposure time was 20 s for H^-, 1,000 s for D^-, 20 s for $^{16}O^-$, 20 s for $^{12}C^{14}N^-$ and 40 s for $^{32}S^-$, respectively. We obtained secondary ion images of $^{12}C^{14}N^-$, $^{12}C^{15}N^-$, $^{12}C^{14}N^-$, $^{12}C^-$, $^{13}C^-$ and $^{12}C^-$ sequentially for the second session after FIB. A 50 μm CA was used for $^{12}C^{14}N^-$, $^{12}C^{15}N^-$, $^{12}C^-$ and $^{13}C^-$ isotopograph. The exposure time was 50 s for $^{12}C^{14}N^-$, 400 s for $^{12}C^{15}N^-$, 50 s for $^{12}C^-$ and 500 s for $^{13}C^-$.

Hydrogen, nitrogen and carbon isotopic composition are represented by δ-value notation;

$$\delta D_{SMOW} = \left\{ \frac{(D/H)_{sample}}{(D/H)_{SMOW}} - 1 \right\} \times 1000$$

$$\delta^{15} N_{AIR} = \left\{ \frac{(^{15}N/^{14}N)_{sample}}{(^{15}N/^{14}N)_{AIR}} - 1 \right\} \times 1000$$

$$\delta^{13} C_{PDB} = \left\{ \frac{(^{13}C/^{12}C)_{sample}}{(^{13}C/^{12}C)_{PDB}} - 1 \right\} \times 1000$$

where SMOW denotes the standard mean ocean water, and AIR denotes the Earth's atmosphere and PDB denotes Pee Dee Belemnite. The instrumental mass fractionations for the D/H, $^{15}N/^{14}N$ and $^{13}C/^{12}C$ ratios of epoxy were corrected by assuming that the δD, $\delta^{15}N$ and $\delta^{13}C$ values are 0‰, respectively, and that the matrix effects are the same for epoxy and organic matters in the UCAMM. Therefore, the δ-values of the organic matters shown here are the relative values to the epoxy. The isotope ratio image was obtained by averaging 5 x 5 pixels (corresponding to 1.0 x 1.0 μm^2) for δD and 3 x 3 pixels (corresponding to 0.6 x 0.6 μm^2) for $\delta^{15}N$ and $\delta^{13}C$ in order to reduce the statistical error. Lateral resolutions of the isotopographs are ~1 μm for $^{1}H^{-}$, and $^{2}D^{-}$ and ~0.6 μm for $^{12}C^{-}$, $^{13}C^{-}$, $^{12}C^{14}N^{-}$, $^{12}C^{15}N^{-}$, $^{32}S^{-}$, and $^{16}O^{-}$.

The morphology of the UCAMM was observed by FE-SEM-EDS (JSM-7000F, Oxford INCA Energy) system at Hokkaido University after the isotope microscope analyses, and a thin section with 200-nm of thickness was prepared by the dual beam focused ion beam and scanning electron microscope (FIB-SEM) JEOL JIB-4501 at Ibaraki University for further analyses.

Carbon (C)-, nitrogen (N)-, and oxygen (O)- X-ray absorption near edge structure (XANES) spectra of the FIB section were acquired by using STXM at the beamline (BL) 5.3.2.2. of Advanced Light Source (ALS) at the Lawrence Berkeley National Laboratory (Kilcoyne et al. 2003). The beamline employs a bending magnet providing a useful photon range spanning approximately from 250 to 800 eV with a flux of 10^{7} photons per second. Energy selection on BL5.3.2 is performed with a low dispersion spherical grating monochromator and affording an energy resolution ($E/\Delta E$) of 5000. Carbon-XANES transmission spectra were obtained in the stack scan mode with 0.1-eV resolution across the near edge region and 0.5-eV resolution below and above the near edge absorption. Energy calibration was conducted by measuring CO_2 and N_2 gas prior to the measurements. The absorption spectra (optical density, OD) were obtained as OD = $-\ln(I/I_0)$, where I is X-ray intensity transmitted from sample and I_0 is that recorded without samples. Leinweber et al. (2007) and Cody et al. (2008) were referred for the absorption peak assignment.

The FIB section was observed under a polarized microscope to check the textural relationships between the MM and the epoxy resin in the section. The section was further observed with a JEOL JEM-2100F field emission TEM, equipped with JEOL JED SDD EDS for detailed textural observation and elemental analysis, at JEOL Corporation and with a JEOL JEM-2100, equipped with an Oxford INCA SDD EDS, at Ibaraki University.

3. Results

3-1. Texture and mineralogy

Figure 1a shows a secondary electron image of an UCAMM D05IB80, which is about ~40 x 30 μm in size. There are abundant sub-μm-sized constituents on the surface of the upper half of this UCAMM. By contrast, the other half is poor in the sub-μm-constituents and has a smooth surface. Ultramicrotomed sections of the UCAMM are shown in Fig. 1b. The sections were selected out of every 3-5 serial sections. There are many mineral grains in the sections No. 1 and 2 (Fig. 1b), which may correspond to the sections of the upper half of the UCAMM shown in Fig. 1a. There are voids in each section, which is composed of densely packed hollow organic material with ~0.5- to ~2-μm thick walls containing minerals.

TEM observation shows that this UCAMM contains glass with embedded metal and sulfide (GEMS) (Figs. 2a, 2b), which is common to the chondritic porous (CS) IDPs (e.g. Bradley and Dai, 2004), UCAMMs previously investigated (Nakamura et al., 2005; Duprat et al., 2010; Dobrică et al., 2012), and CS MMs (Noguchi et al., 2015). Their typical size ranges from ~200 to ~400 nm in diameter and contains tiny (< 30 nm) Fe sulfide as well as rare Fe metal, which appear as S and Fe enriched spots in the elemental distribution maps (Fig. 2c). Oxygen, aluminum, and silicon are homogeneously distributed and magnesium is heterogeneously distributed in the glassy (amorphous silicate) matrix of this GEMS grain (Fig. 2c).

Olivine, low-Ca pyroxene, high-Ca pyroxene, amorphous silica, and pyrrhotite are major inorganic phases in this UCAMM (Figs. 2d-2i), and low-Ca pyroxene and pyrrhotite are more abundant than the other phases. Among these phases, amorphous silica containing no other elements is not common in CP IDPs (e.g. Bradley and Dai, 2004), CP MMs (e. g. Noguchi et al., 2015), and UCAMMs investigated previously (Dobrică et al., 2012). No hydrated silicate was found in the UCAMM.

Major element compositions of olivine, pyroxene, and pyrrhotite in the UCAMM D05IB80 are shown in Fig. 3 and Table 1. Majority of the GEMS grains in this UCAMM are highly depleted in Mg relative to [Si+Al] and Fe and are plotted at the Mg-poor end of the GEMS grains in CP IDPs (Fig. 3a). In addition, sulfur is also depleted in the GEMS grains (Fig. 3b). These data strongly suggest that GEMS grains in this MM do not keep their original chemical compositions.

Olivine is minor in this MM, and the forsterite mol% ranges from ~100 to 89 (Fig. 3c). Low-Ca pyroxene shows a variation of enstatite mol% from ~100 to 78 (Fig. 3c). Because all the high-Ca pyroxene grains analyzed contain high Al_2O_3 contents from 14.7 to 27.8 wt%, they are plotted around the Di apex or outside the pyroxene quadrilateral due to the relative deficiency of Mg^{2+} and Fe^{2+} caused by substitution of Al^{3+} in high-Ca pyroxene (Fig. 3c). FeO vs MnO and FeO vs Cr_2O_3 wt% diagrams show that some low-Ca pyroxene crystals have high MnO (up to 1.85wt%) and high Cr_2O_3 (up to 2.32wt%) contents relative to FeO contents (Figs. 3e, f). Most pyrrhotite crystals are poor in Ni. Only two crystals have 2.8 and 3.2 Ni atomic% (Fig. 3d). These data are consistent with the chemical compositions of olivine, pyroxene, and pyrrhotite in CP IDPs, previously reported UCAMMs, and mineral grains recovered from 81P/Wild 2 (Klöck and Stadermann, 1994; Zolensky and Barrett, 1994; Zolensky et al., 2006, 2008; Joswiak et al., 2009, 2012; Dobrică et al., 2012; Frank et al., 2014).

3-2. Organic material: size, texture, molecular and isotopic compositions

Size

Figure 4 shows the isotopograph of $^{12}C^{14}N^-$, $^{32}S^-$, and $^{16}O^-$ along with the backscattered electron (BSE) image of the UCAMM D05IB80. The distribution of $^{12}C^{14}N^-$ indicates the size of organic carbon is ~ 15 μm × 15 μm. In comparison to the typical size of organic carbon in chondritic meteorites (a few hundreds nm) (e.g., Le Guillou et al., 2014) and that of comet Wild 2 dust particles (~ 1 - 2 μm) (Cody et al. 2008), the organics in the present study is extraordinarily large. $^{32}S^-$ and $^{16}O^-$ are concentrated in the rim of the organic material (Fig. 4), and $^{32}S^-$ is also distributed within the organic material, although its abundance is less than that in the rim.

Observation of soluble organics

UCAMM D05IB80 was originally almost opaque under a transmitted light, though a translucent brown-color part seeped from the sample when it was embedded in epoxy (Fig. 5b). A certain degree of affinity between the UCAMM and epoxy seems to have taken place, which is shown by the observation that the boundary between the embedding epoxy (light brown) and the UCAMM (dark brown) is less clear in the transmitted optical image (Fig. 5d) than in the high-angle annular dark-field scanning transmission electron microscopy (HAADF-STEM) image (Fig. 5e).

Molecular compositions

A Raman spectrum of carbonaceous material in UCAMM D05IB80 is shown in Fig. 6. The spectrum is broad, and the centers and full width at half maximum (FWHM) of D_1 and G are 1338 cm^{-1} (ω_{D1}) and 369 cm^{-1} (Γ_{D1}), and 1569 cm^{-1} (ω_G) and 109 cm^{-1} (Γ_G), respectively. Although the analytical conditions were different from those of the other studies which investigated CP IDPs, MMs, and carbonaceous chondrites (e.g., Rotundi et al., 2008; Busemann et al., 2009; Dobrică et al. 2011; Dartois et al. 2013), the peak broadness and the wave parameters indicate that the carbonaceous material is very disordered.

Combining carbon- and nitrogen-XANES maps of the FIB section, we can distinguish the organic nitrogen-rich regions of the UCAMM from the epoxy that does not contain N (Fig. 7a, b). Nitrogen-XANES spectra of N-rich regions 1 and 2 (Fig. 7d) exhibit intense peaks of 1s-π^* transitions of imine (C=N*) at 398.8 eV (peak E), aromatic nitrogen heterocycles

(C-N*=C) and/or nitrile (C≡N*) at 399.7 eV (peak F), and amide (N*Hx(C=O)C) at ~401.5 eV (peak G). The N-XANES spectra provided a sufficient signal- to-noise (S/N) ratio, which has not been generally observed in chondritic insoluble organic matter and even in organic matter in IDPs (Cody et al. 2011). The relative peak intensity of nitrogen heterocycles in the region 2 is higher than that in the region 1. The nitrogen speciation helps the characterization of carbon functional groups in C-XANES spectra (Fig. 7c). The peak A at ~ 285 eV is assigned to 1s-π* transitions of aromatic/unsaturated carbon (C=C*), which probably includes aromatic nitrogen heterocycles (e.g., pyridine) in the regions 1 and 2, due to the presence of imine in their N-XANES. The peak B at ~286.6 eV are derived from 1s-π* transitions of nitrile/aromatic N or vinyl-keto carbon. The presence of nitrile/aromatic N is very likely because of the intense peaks (peak G) in N-XANES of the regions 1 and 2, while the same peak in the epoxy region would be assigned to vinyl-keto group due to the absence of N. A broad peak ranging 287-288 eV for the regions 1 and 2 includes a peak of 1s-3p/σ* transition to aliphatic carbon (peak C) and a peak D at ~288.3 eV assigned to 1s-π* transitions of carboxyl carbon (C*=O) and/or amidyl carbon (NHx(C*=O)C). The N/C ratio is calculated from the spectral fitting using the aXis 2000 software to be 0.15±0.03, and the O/C ratio is 0.27±0.02, for the region 1. There is a possibility that the XANES results in the present work may be affected by FIB-induced damage, such as an increase of the aromatic carbon (De Gregorio et al. 2010; Bassim et al. 2012). In that case, an original peak intensity of imine may have been relatively lower and those of nitrile and carboxyl groups may have been higher than the acquired spectra. Nevertheless, the possible modification of functional group compositions by FIB should not affect the elemental ratios. Sulfur-XANES measurement was carried out at the BL 5.3.2.1. with a photon energy range of 600-2000 eV, ALS, but the sulfur abundance in the FIB section was below the detection limit of XANES.

Texture

TEM observation of the organic N-rich material reveals the presence of two N-rich regions: the region 1 is smooth and the region 2 is entirely globular (Fig. 8). The two regions are connected at the bottom-left corner of the FIB section (Fig. 5e), indicating that these regions were made of the same organic material as shown in the similar C- and N-XANES spectra (Fig. 7c, d). The globules in the region 2 look similar in size (a few hundred nm) to the organic nanoglobules ubiquitously observed in chondritic meteorites (e.g., Nakamura et al. 2002; Garvie and Buseck, 2004; Nakamura-Messenger et al. 2006; Peeters et al. 2012; De Gregorio et al. 2013; Matsumoto et al. 2013), micrometeorites (Sakamoto et al, 2010), IDPs

(Busemann et al. 2009) and the comet Wild 2 dust particles (De Gregorio et al. 2010; 2011). However, the organic nanoglobules in UCAMM D05IB80, forming aggregates, have more irregular shapes compared to rounded globules in most carbonaceous chondrites. The nanoglobules appear to contain fillings in their interiors (Fig. 8b, c). The high resolution TEM image of the globule filling is shown in Fig. 9(c), which is an aggregate of tiny crystals. Although EDS spectrum of the aggregate suggests that it is composed of low-Ca pyroxene, it was impossible to determine the phase of the crystals due to their small sizes.

TEM images (Fig. 8b, c) revealed that the globular region has three very thin (< 5 nm) surface layers and the smooth region has two (Fig. 8d, e), and the surface layer is less electron-transparent than the interior. The less electron-transparent material is estimated to be amorphous due to the absence of lattice fringes, and is rich in C, O, Si, S, and Fe (Fig. 9), suggesting the presence of silicate and sulfide. High resolution TEM image of the thin layer in the globular region revealed that the layers contain nanocrystals. Although 0.24 and 0.28 nm lattice fringes were observed (Fig. 8f), we could not obtain diffraction spots in the selected area electron diffraction (SAED) patterns, which only gave halo patterns. This is probably due to the minute volumes of these nanocrystals. Therefore, we could not identify phases of these nanocrystals. By contrast, we could not find any nanocrystals at the smooth boundaries (Fig. 8g). The thin layers are thought to be indigenous, and are neither reaction products with epoxy resin nor reaction products with filtrated water in the Antarctica, because the layers is specifically present only in the present UCAMM. If the layers were the secondary products on the Antarctic snow, similar layers should be found in other micrometeorites. The layers are also distinct from a magnetite rim at the surface of micrometeorites formed during heating by atmospheric entry and oxidation (Toppani et al., 2001).

Sodium, K, and Cl are uniformly observed in the smooth region and sporadically in the globular region (Fig. 9). Halite was also identified by XRD (see electronic supplementary data, S2). Although it is difficult to evaluate whether they are indigenous or terrestrial contamination, the homogeneous distributions of these elements as well as N and S do not look like crystal particles of sea salts. The globular region contains a grain consisting of O, Mg, and Si (Fig. 9b). High resolution TEM image of the grain shows that the grain is a polycrystalline aggregate of tiny crystals. 0.46- and 0.24- nm lattice fringes could be assigned as lattice spacing of (200) (~0.46 nm) and (002) (~0.25 nm) of clinoenstatite by considering O, Mg, and Si are major elements (Fig. 9c).

Isotopic compositions

We found no isotopic hot spots in the organic matter in the UCAMMs (Fig. 10). The H, C and N isotopic ratios of the UCAMM D05IB80 are in the range of terrestrial values and not clearly distinguished from those of epoxy ($<2\sigma_{OM}+3\sigma_{epoxy}$). We conclude that the H, C and N isotopic compositions are at the same level as those of terrestrial organics (Fig. 10).

4. Discussion

4-1. Primitive Nature of UCAMM Organics

The highly resolved N-XANES spectra of UCAMM D05IB80 are significantly different from the less characteristic, low signal-to-noise N-XANES spectra of insoluble organic macromolecules (IOM) from chondritic organic materials (e.g., Cody et al., 2008). According to the spectral fitting, the ratio of nitrogen to carbon in the smooth region of the UCAMM organics (N/C = ~0.15) is five times higher than that of insoluble organic macromolecules in types 1 and 2 chondritic meteorites (N/C = ~0.03, Alexander et al. 2007) (Fig. 11). The high nitrogen abundance and most of the identified functional groups (imine C=N, aromatic nitrogen heterocycles C-N=C, nitrile C≡N, amide NHx(C=O)C, and carbonyls COOR) indicate that the UCAMM organic material has high polarity, which indicates its hydrophilic nature and is consistent with the fact that the organic soluble phase was dissolved into epoxy (*i.e.*, polar solvent) (Fig. 5).

In prebiotic organic chemistry, *any* materials become insoluble, tar-like, hydrophobic macromolecules when energy is continuously provided to molecules (Benner et al. 2012). Considering this general chemical phenomema, the nitrogen- and oxygen-bearing polar functional group compositions and the solvent solubility indicate that the UCAMM organic material is extremely primitive compared to those in carbonaceous chondrites.

4-2. Formation of UCAMM Organics and the Role of Small Degree of Aqueous Alteration

Nitrogen-rich and oxygen-bearing complex organic molecules were synthesized by UV photolysis of ices with simulated interstellar/precometary compositions (e.g., H_2O, CH_3OH, CO, NH_3) (e.g., Bernstein et al. 1995; Dworkin et al. 2001; Nuevo et al. 2011), and they were mostly soluble and/or oily (Bernstein et al. 1995; Dworkin et al. 2001; Nuevo et al. 2011) having nanoglobule-like vesicles (Dworkin et al. 2001). The UCAMM in this study shares a chemical similarity to the synthesized organics; UCAMM contains functional groups of nitrile, imine, and amide (Fig. 7d), which were also observed in the photochemical product by Nuevo et al. (2011). The photochemical reaction of ices in the interstellar or pre-stellar environments may have played a role in forming the organic macromolecules in the UCAMM, but the XANES spectrum of the experimentally synthesized organic matter is not completely the same as the present UCAMM. Furthermore, the bulk N/C (= 0.28) and O/C (= 0.51) ratios of the synthesized materials (Nuevo et al. 2011) are much higher than those of the UCAMM. Therefore, photochemistry alone would not be the process responsible for the formation of UCAMM and an additional process(es) would be necessary.

Here we propose that very weak aqueous alteration in the parent body of the UCAMM was responsible for the chemical, structural, mineralogical and morphological characteristics of the UCAMM. Accretion of the organics, ice, submicron-sized mineral particles is a necessary process for forming a certain size of cometary body to retain liquid water, i.e., a meter to kilometer-sized object. In a comet, short-term heating such as planetesimal shock could have locally melted ice grains and released water, which dissolved organic material. Unlike meteorite parent bodies where aqueous fluid mobilizes due to high thermal conductivity with compact mineral structure, it is improbable that aqueous fluid mobilizes in a comet parent body due to very low thermal conductivity of the porous ice structure (40-80% in average) (e.g., Kouchi et al. 1992; Asphaug and Benz, 1996; Farnham and Cochran, 2002;

Kofman et al. 2015). Accordingly, the aqueous fluid on a porous icy body allowed formation of a large sized organic puddle.

Very low degree of melting of ice in a comet or an icy planetesimal causing low mobilization of the fluid well explains the following observations in the present study;

i) Sulfurization of organics. UCAMM D05IB80 contains a considerable amount of sulfur, of which source is easily explained if it was formed in a comet or an icy body. H_2S is a typical component of cometary volatiles (Bockelee-Morvan et al., 2004) and also an aqueous alteration product of sulfide. Thus, the icy parent body of UCAMM D05IB80 may have contained it. Nucleophilic attack of H_2S could have taken place on the partially positive carbonyl carbon of the UCAMM organics (Fig. 7c) and/or their precursor molecule in aqueous fluid. For instance, ketones and aldehydes experimentally gave high yields of organic sulfides ($R\text{-}S_x\text{-}R'$) via a reaction with reduced inorganic sulfur (e.g., HS^-) in aqueous solution at relatively low temperature (20-50°C) for short-duration (e.g., 22 hrs to 4 weeks) (Schouten et al., 1994; van Dongen et al., 2003).

ii) Formation of inorganic nanolayers at the surface of organic material. The organics in UCAMM D05IB80 is covered with a thin inorganic layer as shown in Fig. 8, which can be explained by the adsorption of mineral nanoparticles to an ice-fluid interface. When a fluid was frozen, the partition imbalance of anions and cations between ice and liquid occurs, which is relaxed by the transfer of H^+ and OH^- to each phase, resulting in disproportionate pH between the two phases (Watanabe et al. 2014). The ion-transfer current changes at the interface between organics and salt-bearing ice (Qu et al. 2015). At the interface of two phases with strong contrast of pH and redox-potential, silicate and sulfide membranes osmotically precipitate from the dissolved ions in a fluid (Cairns-Smith, 1982; Russel et al. 1994). The interaction of particles at the ice-fluid interface occurs instantaneously at a cooling rate of -10 ~ -15 K/min from room temperature (Körber et al. 1985). The organic nanoglobules in Tagish Lake meteorite displays similar layers that contain predominantly carbon with minor amounts of O, Si, S, Cl and Fe (Nakamura et al. 2002), which may be also because of the behaviors of ions and mineral particles in a frozen aqueous environment of its parent body.

iii) Formation of irregular-shaped nanoglobule aggregates. The organics in UCAMM D05IB80 shows different textures (smooth and globular textures) (Fig. 8), but their similar chemical compositions suggest simultaneous formation from a common precursor material (Fig. 7). The organic nanoglobules, which would have been originally round, deformed their shapes (e.g., budding) via pH gradient and/or change of osmotic pressure by the generation of the small amount of fluid. For instance, the charge state of an organic molecule changes under different pH, such as a protonated carboxylic acid (R-COOH) at lower pH and an ionized carboxylate ($R\text{-}COO^-$) at higher pH. Vesicles are produced around at neutral pH where the molar ratio of the protonated and ionized forms is equal (e.g., Nawa et al. 2013). However, the fluid in a cometary body could have been basic because of the redistributions of ions (Watanabe et al. 2014) and/or high concentration of NH_3 (Nakamura-Messenger et al. 2011). At the high pH, the vesicles are rapidly deformed (in several seconds) due to dissolution of an ionized form (Nawa et al. 2013). Similarly, textural variations of nanoglobules in insoluble organic residues (De Gregorio et al. 2013; Changela et al. 2013) and matrices (Ivuna, Orgueil and Tagish Lake, see electronic supplementary data, S3) from the aqueous altered carbonaceous chondrites imply the exposure to basic fluid that were generated through the formation of phyllosilicates during the aqueous alteration on their meteorite parent bodies.

4-3. Mineralogical Evidence of Small Degree of Aqueous Alteration

Although GEMS grains in D05IB80 contain Fe-Ni metal and Fe sulfide tiny crystals (Fig. 2), they are rarer than those in GEMS in CP IDPs (e. g. Keller and Messenger, 2011) and CP MMs (Noguchi et al. 2015). Mg in the amorphous silicate in GEMS grains are heterogeneously distributed and on average highly depleted (Fig. 2c). By contrast, Si is enriched in the Mg-depleted areas in GEMS (Fig. 2c). Heterogeneous distribution of Si and Mg within each GEMS grain in IDPs has already been reported (e.g., Keller and Messenger, 2011). In the case of D05IB80, Si-rich areas are predominant and amorphous silicate is enriched in Fe (Figs. 2, 3).

Because Fe-Ni metal is among the first phase to alter by aqueous alteration (Zolensky et al. 1993; Hanowski and Brearley 2000, 2001; Chizmadia et al. 2008), the rarity of nano Fe metal in GEMS indicates a slight degree of aqueous alteration. It has been already reported that rare Fe-Ni metal phases were found from the UCAMMs and their GEMS-like objects collected by the French-Italian team (Dobrică et al. 2012). The depletion of metal may be a common feature of UCAMMs. The GEMS grains with rare nanophase Fe metal particles in the Acfer 094 carbonaceous chondrite (Vollmer et al., 2009a, b) have been thought to be the results of oxidation of Fe metal due to nascent aqueous alteration of the amorphous silicates (Keller et al. 2009). Le Guillou and Brearley (2014) reported the absence of metal grains associated with the amorphous silicate material in MET 00426 CR3 chondrite, and discussed that the absence was due to hydration of the amorphous silicate.

In the case of D05IB80, nano Fe sulfide is also depleted in GEMS. It does not necessarily mean that D05IB80 experienced slightly higher degrees of aqueous alteration than the primitive meteorites because hydrous phyllosilicates are not identified in the UCAMM. A slightly oxidizing condition of aqueous alteration might have promoted dissolution of nano Fe sulfide in GEMS of the UCAMM.

There is no Ni-bearing pyrrhotite in the UCAMM (< 3.2 atomic% Ni) (Fig. 3d), which is consistent with the idea that the UCAMM experienced very weak aqueous alteration. The minimal degree of aqueous alteration is also consistent with that aqueous alteration products were not found on olivine and pyroxene (Fig. 6).

Based on the chemical and mineralogical features described above, we conclude that the UCAMM experienced a very weak degree of aqueous alteration on a cometary nucleus or an icy asteroid, which are not seen on the typical types 1 and 2 chondritic meteorite parent bodies. Possible heat source for the generation of liquid water in icy small bodies is i) short-lived radioactive nuclides, ii) perihelion passage (Nakamura-Messenger et al. 2011), iii) collisions of planetesimals (Cody et al. 2011), or iv) reduction of the freezing point by the presence of solutes, e.g., ammonia (Pizzarello et al. 2011) and methanol.

The condition of aqueous alteration of the UCAMM can be estimated by the experiments by Nakamura-Messenger et al. (2011). They have conducted a hydrothermal experiment of anhydrous IDPs and reported the rapid formation of hydrated silicates at 25-160°C for 12-24 hours under basic pH conditions (pH=12), that is, alteration of amorphous silicate into hydrous phyllosilicate possibly proceeds extremely quickly. UCAMM DO05IB80 does not contain hydrous silicates but Mg and S leached out from GEMS grains instead, which indicates a shorter duration reaction at lower temperature, lower pH and/or slightly oxidizing conditions compared to their experiments. Considering that the degree of alteration should have been much lower than aqueous alteration in the major CM and CI carbonaceous chondrites that lasted for several million years (e.g., Fujiya et al. 2013), planetesimals collisions are most likely to produce a very weak degree of aqueous alteration in a short duration. The large $P\varDelta V$ irreversible energy deposition during compaction of pore spaces of cometary ices initiates melting at very low shock pressures of 0.1-0.5 GPa between 250 and 150K (Stewart and Ahrens, 2004). The pressure range is comparable to the typical impact velocities of comets generating the peak pressures of ~1 GPa (Stewart and Ahrens, 2004).

Although there may be a possibility that the UCAMM had suffered terrestrial weathering in Antarctic snow, the possibility would be low because iron hydroxide, which is easily formed by weathering of pyrrhotite (Taylor et al. 2002), is not identified. The residence time of the micrometeorites at the Antarctic snow is much shorter (ca. a year) than the lifetime of the Antarctic ice (ca. thousands years), and the average temperatures near the Dome Fuji station is -54°C (Shiraishi, 2012), which would prevent the weathering reaction.

4-4. Comparison with Other UCAMMs, AMMs, IDPs, Comets, and Chondritic Meteorites

UCAMM D05IB80 consists of large (tens of micrometers) organic material with submicron-sized mineral species such as crystalline silicate, sulfide, and GEMS grains. Similarly, UCAMMs investigated by Duprat et al. (2010) and Dobrică et al. (2012) have continuous large areas composed of carbonaceous material, and minerals and GEMS grains are embedded in the carbonaceous material. The nitrogen chemical characteristics of organic material in the UCAMM D05IB80 is consistent with those described by Dartois et al. (2013), who identified C=N and C≡N from their non-FIB UCAMM samples. The similarity suggests that the organic chemistry and mineralogy identified in the present study are common for UCAMMs, although GEMS grains in their UCAMMs are enriched in Fe sulfide nanocrystals and do not show depletion of Mg and S.

The isotopic compositions of UCAMMs appear to be highly variable; D, ^{13}C, and ^{15}N isotopic compositions are normal in this study, which is also the case for a UCAMM containing abundant presolar grains (Floss et al., 2012). On the contrary, extreme enrichments of D and ^{15}N are found in two UCAMMs by the French-Italian team (Duprat et al. 2010; Dartois et al. 2013). Duprat et al. (2010) showed that one UCAMM had an area of larger D excess ($\delta D >$ ～10000‰) than another ($\delta D >$ 5400‰) with a clear boundary. Indeed, the stratosphere IDPs (Messenger, 2000) and the comet Wild 2 dust particles (Matrajt et al. 2012) show a wide range of the H and N isotopic compositions from values extremely rich in heavy-isotopes to normal values with the terrestrial levels. Thus, it is difficult to determine the origin of the samples only with the presence or absence of the isotopic anomalies.

An anhydrous interplanetary dust particle (IDP) L2006LB23 is comprised mainly of carbonaceous material (~90%) (Thomas et al. 1994). The IDP is regarded as an ultracarbonaceous IDP. The ultramicrotomed section (Figs. 1 and 2 in Thomas et al. 1994) has a bubble-wall structure made by organic material containing minerals grains, which is quite similar to the sections of the UCAMM D05IB80. Not only the internal structure, but also mineralogy of the ultracarbonaceous IDP is similar to the UCAMM D05IB80. The IDP contains Si-rich glass containing Fe sulfide and Fe-Ni metal grains, Si-rich glass, pyroxene, olivine, and Fe sulfide. In addition to pyroxene, olivine, and Fe sulfide, the UCAMM D05IB80 contains amorphous SiO_2 and GEMS grains that are highly depleted in Mg and S

(Figs. 2, 3). It is likely that these two phases correspond to Si-rich glass and Si-rich glass containing Fe sulfide and Fe-Ni metal grains in L2006LB23. These data suggest that there is a genetic relationship between these objects.

Mineralogy and nitrogen-rich organic functional group chemistry were common to the UCAMM D05IB80 and one of the anhydrous AMMs (D10IB009) collected from the Antarctic snow near Dome Fuji station (Noguchi et al. 2017). On the other hand, a difference is that D10IB009 contains GEMS including Fe-metal, and thus it is likely that the UCAMM D05IB80 is aqueously more altered than the anhydrous AMM. Another difference is that the organic material in D10IB009 has D- and ^{15}N-enrichments (δD = ~2000-10000‰, δ^{15}N = ~300-1000‰) (Noguchi et al. 2017), similarly to CP-IDPs (e.g., Messenger et al. 2000), although it is unlikely that the lack of isotopic anomalies in the UCAMM be due to the aqueous alteration, based on the facts that a number of aqueous altered carbonaceous chondrites retain organics enriched in the heavy isotopes (e.g., Busemann et al. 2006; Nakamura-Messenger et al. 2006; Hashiguchi et al. 2013).

It should be noted that the N-XANES spectra of the regions 1 and 2 in the UCAMM D05IB80 (Fig. 7d) are very similar to those of three particles of comet Wild 2 with N/C ratios of 0.08-0.16, one of which was an organic nanoglobule with the nitrogen isotopic composition indistinguishable from the terrestrial values (De Gregorio et al., 2010). Other particles of comet Wild 2 have lesser amounts of imine, nitrile, and amidyl groups than amino, urea, and carbamoyl (NHx(C=O)OR) groups in their N-XANES spectra (Cody et al., 2008), but the N/C (~ 0.12) and O/C (0.22 – 0.28) ratios of some of the spectra are comparable to those in this study (Fig. 11). Moreover, the appearance of the organic soluble phase in UCAMM D05IB80 extracted from epoxy (Fig. 5) is similar to those of the epoxy-soluble organic matter in the comet Wild 2 dust particles (Cody et al. 2008; De Gregorio et al. 2011).

The chemical and isotopic characteristics of UCAMM-D05IB90 are significantly different from the organic materials in types 1 and 2 carbonaceous chodrites (e.g., Cody et al., 2011), while they are similar to some of the primitive CR3 chondrites. The large smooth organic material connected with globular organics in the UCAMM is similar to that in a CR3 chondrite, MET 00426, observed by Le Guillou and Brearley (2014), which is an elongated vein 3–4 μm in length and up to 1 μm width, with a sharp boundary between surrounding silicates and sulfides. They observed a single organic nanoglobule embedded in the main organic mass and an aggregate of rounded particles connected to the main vein. Peeters et al. (2012) also found a several micron-sized organic vein containing a number of nanoglobules in QUE 99177 CR3 chondrite, of which N-XANES spectrum is similar to our observation. The comet Wild 2 is estimated to have experienced little or no aqueous alteration on the basis of the absence of phyllosilicates (Zolensky et al. 2006). CR3 chondrites contain abundance amorphous silicates (e.g., Abreu and Brearley, 2010; Le Guillou and Brearley, 2014) and are thought to have experienced the earliest stage of parent body aqueous alteration. Therefore, the similarities among the organics in the UCAMM D05IB80, the comet Wild 2, and CR3 chondrites corroborate that the UCAMM are more primitive than most of the aqueously-altered carbonaceous chondrites.

The recent results by the Rosetta mission unveiled the presence of organic-rich, dark dehydrated surface of the comet 67P/Churyumov-Gerasimenko by the Visible, Infrared and Thermal Imaging Spectrometer (VIRTIS) (Capaccioni et al. 2015). The evolved gas analyzer Cometary Sampling and Composition (COSAC) mass spectrometry identified a number of nitrogen-bearing organic molecules, such as nitriles, amines, amides, and isocyanates, but no sulfur species on the comet 67P/C-G (Goesmann et al. 2015). The high abundance and chemical compositions of organics on the comet 67P/Churyumov-Gerasimenko may be related to the precursor material of large N-rich organics of the UCAMM, prior to organic sulfurization under aqueous condition.

Moreover, our work reports the first finding of organic materials retaining C, H, O, N and

S elements all together from micrometeorites. Another finding of CHONS organics has been reported from the polar solvent extracts from Murchison meteorite (Schmitt-Kopplin et al. 2010). Because of the unusual similarity in the organic elemental compositions and polar nature between the UCAMM and Murchison, the possibility that the UCAMM organics contains the precursor of the meteoritic CHONS compounds is expected, and could be a key indicator of the comet-asteroid continuum. In order to trace back and determine the precursors of organic materials in the early Solar System, further analyses and comparative studies of the most primitive extraterrestrial materials we can obtain, such as anhydrous micrometeorites, IDPs and the least altered carbonaceous chondrites through the comprehensive inorganic and organic analytical strategies without discrimination between soluble and insoluble, will be necessary.

5. Summary

An ultracarbonaceous micrometeorite (UCAMM D05IB80), collected from near the Dome Fuji Station, Antarctica, has been investigated by coordinated *in-situ* analyses. According to the following unique features of organics and minerals that are different from chondritic meteorites, we conclude that the UCAMM was formed by small amount of fluid-induced interaction of organics and minerals in a porous ice-rich cometary body.

1. A major part of the organic materials in the UCAMM shows a smooth texture to which globular aggregates are connected, and includes an epoxy-soluble phase. The UCAMM shows nitrogen-rich organic chemistry (N/C = 0.15). Its organic functional groups include a variety of nitrogen-bearing groups; heterocyclic nitrogen, nitrile, imine, and amide. The polar functional group compositions and the solvent solubility indicate very primitive nature of the organic material in the UCAMM.
2. GEMS grains are depleted in Mg and S. This is an evidence for incipient aqueous alteration in the UCAMM parent body. Shock heating in an icy planetesimal instantaneously melted ice grains and released water, which dissolved organic material. Due to the high porosity and low density of a cometary body, the fluid did not diffuse but formed a large-size organic puddle (15 x 15 μm). The locally generated fluid sulfurized organic material, formed mineral thin layers (C, O, Si, S, and Fe) at the surface of organics, and deformed the shape of organic nanoglobules.

Acknowledgements

We appreciate Christine Floss, anonymous reviewer, and associate editor Eric Quirico for their constructive comments and helpful editorial handling. This work is supported by a Grant-in-Aid for Scientific Research from the Japanese Ministry of Education, Culture, Sports, Science and Technology (No. 22224010, PI: H. Nagahara). The STXM facility at the beamline 5.3.2.2, ALS, is supported by the Department of Energy, Basic Energy Sciences program.

References

Abreu N. M. and Brearley A. J. (2010) Early solar system processes recorded in the matrices of two highly pristine CR3 carbonaceous chondrites, MET 00426 and QUE 99177. *Geochim. Cosmochim. Acta* **74**, 1146– 1171.

Alexander C. M. O'D., Fogel M., Yabuta H. and Cody G. D. (2007) The origin and evolution of chondrites recorded in the elemental and isotopic compositions of their macromolecular organic matter. *Geochim. Cosmochim. Acta* **71**, 4380– 4403.

Asphaug E. and Benz W. (1996) Size, Density, and Structure of Comet Shoemaker–Levy 9 Inferred from the Physics of Tidal Breakup. *Icarus* **121**, 225-248.

Bassim N. D., De Gregorio B. T., Kilcoyne A. L. D., Scott K., Chou T., Wirick S., Cody G. and Stroud R. M. (2012) Minimizing damage during FIB sample preparation of softmaterials. *J. Microscopy* **245**, 288–301.

Benner S. A., Kim, H-J. and Carrigan M.A. (2012) Asphalt, water, and prebiotic synthesis of ribose, ribonucleosides, and RNA. *Acc. Chem. Res.* **45**, 2025-2034.

Bernstein M. P., Sandford S. A., Allamandola L. J., Chang S. and Scharberg M. A. (1995) Organic Compounds Produced by Photolysis of Realistic Interstellar and Cometary Ice Analogs Containing Methanol. *Astrophys. J.* **454**, 327–344.

Bockelée-Morvan D., Crovisier J., Mumma M. J., and Weaver H. A. (2004) The composition of cometary volatiles. In Comets II (eds. Festou M. C., Keller H. U., and Weaver H. A.) Tucson, AZ: The University of Arizona Press. pp. 391–423.

Bradley J. P. and Brownlee D. E. (1986) Cometary particles: Thin sectioning and electron beam analysis. *Science* **231**, 1542-1544.

Bradley J. P. and Dai Z. R. (2004) Mechanism of formation of glass with embedded metal and sulfides. *The Astrophysical Journal* **617**, 650-655.

Bradley J. P., Keller L. P., Snow T. P., Hanner M. S., Flynn G. J., Gezo J. C., Clemett S. J., Brownlee D. E. and Bowey J. E. (1999) An infrared spectral match between GEMS and interstellar grains. *Science* **285**, 1716-1718.

Busemann H., Young A. F., Alexander C. M. O'D., Hoppe P., Mukhopadhyay S. and Nittler

L. R. (2006) Interstellar chemistry recorded in organic matter from primitive meteorites. *Science* **314**, 727–730.

Busemann H., Nguyen A. N., Cody G. D., Hoppe, P., Kiloyne, A. L. D., Stroud, R. M., Zega T. J. and Nittler L. R. (2009) Ultra-primitive interplanetary dust particles from the comet 26P/Grigg–Skjellerup dust stream collection. *Earth Planet. Sci. Lett.* **288**, 44–57.

Cairns-Smith A. G (1982) Genetic takeover and the mineral origins of life. Cambridge University Press, Cambridge, England.

Capaccioni, F., Coradini, A., Filacchione, G., et al. (2015) *Science* **349**, aab0628-1-aab0628-4.

Changela H. G., Cody G. D., Alexander C. M. O'D., Nittler L. R., Peeters Z., De Gregorio B. T. and Stroud R. M. (2013) TEM Study of insoluble organic matter in primitive chondrites: Unusual textures associated with organic nanoglobules. *Lunar Planet. Sci.* **XLIV**, #3101.

Chizmadia L. J., Xu Y., Schwappach C. and Brearley A. J. (2008) Characterization of micron-sized Fe,Ni metal grains in fine-grained rims in the Y-791198 CM2 carbonaceous chondrite: Implications for asteroidal and preaccretionary models for aqueous alteration. *Meteor. Planet. Sci.* **43**, 1419–1438.

Cody G. D., Ade H., Alexander C. M. O'D., Araki T., Butterworth A., Fleckenstein H., Flynn G., Gilles M. K., Jacobsen C., Kilcoyne A. L. D., Messenger K., Sandford S. A., Tyliszczak T., Westphal A. J., Wirick S. and Yabuta H. (2008) Quantitative organic and light-element analysis of comet 81P/Wild 2 particles using C-, N-, and O- XANES. *Meteor. Planet. Sci.* **43**, 353–365.

Cody G. D., Heying E., Alexander C. M. O. D., Nittler L. R., Kilcoyne A. L. D., Sandford S. A. and Stroud R. M. (2011) Establishing a molecular relationship between chondritic and cometary organic solids. *Proc. Natl. Acad. Sci. USA* **108**, 19171–19176.

Dartois E., Engrand C., Brunetto R., Duprat J., Pino T., Quirico E., Remusat L., Bardin N., Briani G., Mostefaoui S., Morinaud G., Crane B., Szwec N., Delauche L., Jamme F., Sandt Ch. and Dumas P. (2013) Ultracarbonaceous Antarctic micrometeorites, probing the Solar System beyond the nitrogen snow-line. *Icarus* **224**, 243–252.

De Gregorio B. T., Stroud R. M., Nittler L. R., Alexander C. M.O'D., Kilcoyne A. L. D. and Zega T. J. (2010) Isotopic anomalies in organic nanoglobules from Comet 81P/Wild 2: Comparison to Murchison nanoglobules and isotopic anomalies induced in terrestrial organics by electron irradiation. *Geochim. Cosmochim. Acta* **74**, 4454-4470.

De Gregorio B. T., Stroud R. M., Cody G. D., Nittler L. R., Kilcoyne A. L. D. and Wirick S.

(2011) Correlated microanalysis of cometary organic grains returned by Stardust. *Meteor. Planet. Sci.* **46**, 1376-1396.

De Gregorio B. T., Stroud R. M., Nittler L. R., Alexander C. M.O'D., Bassim N. D., Cody G. D., Kilcoyne A. L. D., Sandford S. A., Milam S. N., Nuevo M. and Zega T. J. (2013) Isotopic and chemical variation of organic naoglobules in primitive meteorites. *Meteor. Planet. Sci.* **48**, 904-928.

Dobrica˘ E., Engrand C., Quirico E., Montagnac G. and Duprat J. (2011) Raman characterization of carbonaceous matter in CONCORDIA Antarctic micrometeorites. *Meteor. Planet. Sci.* **46**, 1363-1375.

Dobrica˘ E., Engrand C., Leroux H., Rouzaud J.-N. and Duprat J. (2012) Transmission electron microscopy of CONCORDIA ultracarbonaceous Antarctic micrometeorites (UCAMMs): Mineralogical properties. *Geochim. Cosmochim. Acta* **76**, 68–82.

Duprat J., Dobrica E., Engrand C., Aléon J., Marrocchi Y., Mostefaoui, S., Meibom A., Leroux H., Rouzaud J.-N., Gounelle M., Robert F. (2010) Extreme deuterium excesses in ultracarbonaceous micrometeorites from central Antarctic snow. *Science* **328**, 742-745.

Dworkin J. P., Deamer D. W., Sandford S. A. and Allamandola L. J. (2001) Self-assembling amphiphilic molecules: Synthesis in simulated interstellar/precometary ices. *Proc. Natl.*

Acad. Sci. USA **98**, 815-819.

Farnham T. L. and Cochran A. L. (2002) A McDonald Observatory Study of Comet 19P/Borrelly: Placing the Deep Space 1 Observations into a Broader Context. *Icarus* **160**, 398-418.

Floss C., Noguchi T. and Yada T. (2012) Ultracarbonaceous Antarctic micrometeorites: Origins and relationships to other primitive extraterrestrial materials. *Lunar Planet. Sci.* **XLIII**, #1217.

Floss C., Stadermann F. J., Bradley J., Dai Z. R., Bajt S., and Graham G. (2004) Carbon and nitrogen isotopic anomalies in an anhydrous interplanetary dust particle. *Science* **303**, 1355-1358.

Frank D. R., Zolensky M. E. and Le L. (2014) Olivine in terminal particles of Stardust aerogel tracks and analogous grains in chondrite matrix. *Geochim. Cosmochim. Acta* **142**, 240–259.

Fujiya W., Sugiura N., Sano Y. and Hiyagon H. (2013) Mn–Cr ages of dolomites in CI chondrites and the Tagish Lake ungrouped carbonaceous chondrite. *Earth Planet. Sci. Lett.* **362**, 130–142.

Garvie L. A. J. and Buseck P. R. (2004) Nanosized carbon-rich grains in carbonaceous chondrite meteorites. *Earth Planet. Sci. Lett.* **224**, 431–439.

Goesmann F., Rosenbauer H., Bredehoft J. H., Cabane M., Ehrenfreund P., Gautier T., Giri Chaitanya, Kruger H., Le Roy L., MacDermott A. J., McKenna-Lawlor S., Meierhenrich U. J., Munoz Caro G. M., Raulin F., Roll R., Steele A. Steininger H., Sternberg R., Szopa C., Thiemann W. and Ulamec S. (2015) Organic compounds on comet 67P/Churyumov-Gerasimenko revealed by COSAC mass spectrometry. *Science* **349**, aab0689-1- aab0689-3.

Greenberg J. M. and Li A. (1997) Silicate core-organic refractory mantle particles as interstellar dust and as aggregated in comets and stellar disks. *Adv. Space Res.* **19**, 981–990.

Hanowski N. P. and Brearley A. J. (2000) Iron-rich aureoles in the CM carbonaceous chondrites, Murray, Murchison and ALH81002: Evidence for in situ alteration. *Meteor. Planet. Sci.* **35**, 1291–1308.

Hanowski N. P. and Brearley A. J. (2001) Aqueous alteration of chondrules in the CM carbonaceous chondrites, Allan Hills 81002. *Geochim. Cosmochim. Acta* **65**, 495–518.

Hashiguchi M., Kobayashi S. ad Yurimoto H. (2013) In situ observation of D-rich carbonaceous globules embedded in NWA 801 CR2 chondrite. *Geochim. Cosmochim.*

Acta **122**, 306-323.

Joswiak D. J., Brownlee D. E., Matrajt G., Westphal A. J. and Snead C. J. (2009) Kosmochloric Ca-rich pyroxenes and FeO rich olivines (Kool grains) and associated phases in Stardust tracks and chondritic porous interplanetary dust particles: possible precursors to FeO-rich type II chondrules in ordinary chondrites. *Meteorit. Planet. Sci.* **44**, 1561–1588.

Joswiak D. J., Brownlee D. E., Matrajt G., Westphal A. J., Snead C. J. and Gainsforth Z. (2012) Comprehensive examination of large mineral and rock fragments in Stardust tracks: mineralogy, analogous extraterrestrial materials, and source regions. *Meteorit. Planet. Sci.* **47**, 471–524.

Keller L. P. and Messenger S. (2011) On the origins of GEMS grains. *Geochim. Cosmochim. Acta* **75**, 5336–5365.

Keller L. P., Nakamura-Messenger K. and Messenger S. (2009) Amorphous silicates in primitive meteoritic materials: Acfer 094 and IDPs. 72nd Annual Meteoritical Society Meeting 44. #5371 (abstract).

Kilcoyne A. L. D., Tyliszczak T., Steele W. F., Fakra S., Hitchcock P., Franck K., Anderson E., Harteneck B., Rightor E. G., Mitchell G. E., Hitchcock A. P., Yang L.,Warick T. and

Ade, H. (2003) Interferometer controlled scanning transmission microscopes at the Advanced Light Source. *J. Synchrotron Rad.* **10**, 125–136.

Klöck W. and Stadermann F. J. (1994) Mineralogical and chemical relationships of interplanetary dust particles, micrometeorites and meteorites. In Analysis of Interplanetary Dust (eds. M. E. Zolensky et al.,), pp. 51–87. AIP Conference Proceedings 310, New York.

Kofman et al. (2015) Properties of the 67P/Churyumov-Gerasimenko interior revealed by CONSERT radar. Science **349**, aab0639-1 – aab0639-6.

Körber C., Rau G., Cosman M. D. and Cravalho E. G. (1985) Interaction of particles and a moving ice-liquid interface. *J. Cryst Growth* **72**, 649-662.

Kouchi A., Greenberg J. M., Yamamoto T., and Mukai T. (1992) Extremely low thermal conductivity of amorphous ice: relevance to comet evolution. *Astrophys. J.* **388**, L73-L76.

Le Guillou C. and Brearley, A. J. (2014) Relationships between organics, water and early stages of aqueous alteration in the pristine CR3.0 chondrite MET00426. *Geochim. Cosmochim. Acta*, **131**, 344-367.

Le Guillou C., Bernard S., Brearley, A. J. and Remusat L. (2014) Evolution of organic matter in Orgueil, Murchison and Renazzo during parent body aqueous alteration: *In situ* investigations. *Geochim. Cosmochim. Acta*, **131**, 368-392.

Leinweber P., Kruse J., Walley F. L., Gillespie A., Eckhardt K-U., Blyth R. I. R. and Regier T. (2007) Nitrogen K-edge XANES – an overview of reference compounds used to identify 'unknown' organic nitrogen in environmental samples. *J. Synchrotron Rad.* **14**, 500–511.

Matrajt G., Messenger S., Brownlee D. and Joswiaki D. (2012) Diverse forms of primordial organic matter identified in interplanetary dust particles. *Meteor. Planet. Sci.* **47**, 525-549.

Matsumoto T., Tsuchiyama, A., Nakamura-Messenger, K., Nakano, T., Uesugi, K., Takeuchi, A. and Zolensky, M. E. (2013) Three-dimensional observation and morphological analysis of organic nanoglobules in a carbonaceous chondrite using X-ray micro-tomography. *Geochim. Cosmochim. Acta* **116**, 84-95.

Messenger S. (2000) Identification of molecular-cloud material in interplanetary dust particles. *Nature* **404**, 968-971.

Messenger, S., Sandford, S. and Brownlee, D. (2006) The population of starting materials available for Solar System construction. *In: Meteorites and the Early Solar System II* (eds. Lauretta D. S. and McSween, H. Y., Jr.) Univ. of Arizona, USA, pp. 187-208.

Nakamura K., Zolensky M. E., Tomita S., Nakashima S. and Tomeoka K. (2002) Hollow organic globules in the Tagish Lake meteorite as possible products of primitive organic reactions. *International Journal of Astrobiology* **1**, 179-189.

Nakamura T., Noguchi T., Ozono Y., Osawa T. and Nagao K. (2005) Mineralogy of ultracarbonaceous large micrometeorites. *Meteor. Planet. Sci.* **40**, A110.

Nakamura-Messenger K., Messenger S., Keller L. P., Clemett S. J. and Zolensky M. E. (2006) Organic globules in the Tagish Lake meteorite: remnants of the protosolar disk. *Science* **314**, 1439– 1442.

Nakamura-Messenger K., Clemett S. J., Messenger S. and Keller L. P. (2011) Experimental aqueous alteration of cometary dust. *Meteor. Planet. Sci.* **46**, 843–856.

Nawa E., Nishigaki Y., Yamamoto D. and Shioi A. (2013) Rhythmic shape change of a vesicle under a pH gradient. *Soft Matter* **9**, 7832-7842.

Noguchi T., Ohashi N., Tsujimoto S., Mitsunari T., Bradley J. P., Nakamura T., Toh S., Stephan T., Iwata N. and Imae N. (2015) Cometary dust in Antarctic ice and snow: Past and present chondritic porous micrometeorites preserved on the Earth’s surface. *Earth Planet. Sci. Lett.* **410**, 1-11.

Noguchi T., Yabuta H., Itoh S., Sakamoto N., Mitsunari T., Okubo A., Okazaki R., Nakamura

T., Tachibana S., Terada K., Ebihara M., Imae N., Kimura M. and Nagahara H. (2017) Variation of mineralogy and organic material during the early stages of aqueous activity recorded in Antarctic micrometeorites. *Geochim. Cosmochim. Acta* **208**, 119–144.

Nuevo M., Milam S. N., Sandford S. A., De Gregorio B. T., Cody G. D. and Kilcoyne A.L.D. (2011) XANES analysis of organic residues produced from the UV irradiation of astrophysical ice analogs. *Adv. Space Res.* **48**, 1126–1135.

Peeters Z., Changela H. G., Stroud R. M., Alexander C. M. O'D. and Nittler L. R. (2012) Coordinated analysis of in situ organic material in the CR chondrite QUE 99177. *Lunar Planet. Sci.* **XLIII**, #2612.

Pizzarello S. Williams L. B., Lehman J., Holland G. P. and Yarger J. L. (2011) Abundant ammonia in primitive asteroids and the case for a possible exobiology. *Proc. Nat. Acad. Sci. USA* **108**, 4303-4306.

Qu H., Harada M. and Okada T. (2015) Ion-transfer voltammetry at the interface between organic and salt-doped ice phases. *ChemElectroChem* **2**, 1249-1253.

Rotundi A., Baratta G. A., Borg J., Brucato J. R., Busemann H., Colangeli L., d'Hendecourt L., Djouadi Z., Ferrini G., Franchi I. A., Fries M., Grossemy F., Keller L. P., Mennella V., Nakamura K., Nittler L. R., Palumbo M. E., Sandford S. A., Steele, A. and Wopenka, B.

(2008) Combined micro-Raman, micro-infrared, and field emission scanning electron microscope analyses of comet 81P/Wild 2 particles collected by Stardust. *Meteorit. Planet. Sci.* **43**, 367–397.

Russell M. J., Daniel R. M., Hall A. J. and Sherringham J. A. (1994) A hydrothermally precipitated catalytic iron sulphide membrane as a first step toward life. *J. Mol. Evol.* **39**, 231-243.

Sakamoto K., Nakamura T., Noguchi, T. and Tsuchiyama, A. (2010) A new variant of saponite-rich micrometeorites recovered from recent Antarctic snowfall. *Meteorit. Planet. Sci.* **45**, 220–237.

Schmitt-Kopplin P., Gabelica Z., Gougeon R. D., Fekete A., Kanawati B., Harir M., Gebefuegi I., Eckel G. and Hertkorn N. (2010) High molecular diversity of extraterrestrial organic matter in Murchison meteorite revealed 40 years after its fall. *Proc. Natl. Acad. Sci. USA* **107**, 2763–2768.

Schouten S., de Graaf W., Sinninghe Damsté J. S., van Driel G. B., de Leeuw J. W. (1994) Laboratory simulation of natural sulphurization: II. Reaction of multi-functionalized lipids with inorganic polysulphides at low temperatures. *Org. Geochem.* **22**, 825-834.

Shiraishi K. (2012) Dome fuji station in east antarctica and the Japanese antarctic research expedition. *Proceedings of the International Astronomical Union* **8**, 161-168.

Stewart S. T. and Ahrens T. J. (2004) A new H_2O ice Hugoniot: Implications for planetary impact events. *AIP Conf. Proc.* **706**, 1478-1483.

Taylor L. A., Nazarov M. A., Shearer C. K., McSween H. Y., Cahill J., Neal C. R., Ivanova M. A., Barsukova L. D., Lentz R. C., Clayton R. N. and Mayeda T. K. (2002) Martian meteorite Dhofar 019: A new shergottite. *Meteor. Planet. Sci.* **37**, 1107–1128.

Thomas K., Keller L.P., Blanford G. E. and McKay D. S. (1994) Quantitative analyses of carbon in anhydrous and hydrated interplanetary dust particles. in: Analysis of interplanetary dust, (M. E. Zolensky, T. L. Wilson, F. J. M. Rietmeijer, G. J. Flynn eds), 165-172.

Toppani A., Libourel G., Engrand C. and Maurette M. (2001) Experimental simulation of atmospheric entry of micrometeorites. *Meteor. Planet. Sci.* **36**, 1377-1396.

van Dongen B. E., Schouten S., Baas M., Geenevasen J. A. J. and Sinninghe Damsté J. S. (2003) An experimental study of the low-temperature sulfurization of carbohydrates. *Org. Geochem.* **34**, 1129–1144.

Vollmer C., Brenker F. E., Hoppe P. and Stroud R. M. (2009a) Direct laboratory analysis of silicate stardust from rRed giant stars. *Astrophys. J.* **700**, 774–780.

Vollmer C., Hoppe P., Stadermann F. J., Floss C. and Brenker F. E. (2009b) NanoSIMS analysis and Auger electron spectroscopy of silicate and oxide stardust from the carbonaceous chondrite Acfer 094. *Geochim. Cosmochim. Acta* **73**, 7127–7149.

Watanabe H., Otsuka T., Harada M. and Okada T. (2014) Imbalance between anion and cation distribution at ice interface with liquid phase in frozen electrolyte as evaluated by fluorometric measurements of pH. J. Phys. Chem. C. **118**, 15723-15731.

Yada T., Floss C., Stadermann F. J., Zinner E., Nakamura T., Noguchi T. and Lea S. (2008) Stardust in Antarctic micrometeorites. *Meteorit. Planet. Sci.* **43**, 1287-1298.

Yurimoto H., Nagashima K. and Kunihiro T. (2003) High precision isotope micro-imaging of materials. *Appl. Surf. Sci.* **203-204**, 793-797.

Zolensky M. E., Barrett B. and Browning L. (1993) Mineralogy and composition of matrix and chondrule rims in carbonaceous chondrites. *Geochim. Cosmochim. Acta* **57**, 3123–3148.

Zolensky M. E. and Barrett R. A. (1994) Composition variations of olivines and pyroxenes in chondritic interplanetary dust particles. *Meteoritics* **29**, 616–620.

Zolensky M. et al. (2006) Mineralogy and petrology of comet Wild 2 nucleus samples. *Science* **314**, 1735–1739.

Figure captions:

Figure 1. (a) Secondary electron image of an ultracarbonaceous micrometeorite (UCAMM) D05IB80 placed on a platinum plate. The upper half of the UCAMM is porous and covered by fine-grained (typically sub μm) particles, whereas the lower half is smooth. (b) Bright-field (BF) TEM images of ultramicrotomed sections of the UCAMM D05IB80. Each section was selected out of every three to five serial sections. Abbreviations: LPx , low-Ca pyroxene; PO, pyrrhotite; Ol, Olivine.

Figure 2. (a, b) BF-TEM images of GEMS grains in the UCAMM D05IB80. (c) HAADF-STEM image and elemental distribution maps of the same GEMS grains in (b). (d-i) BF TEM images of minerals in a FIB section and ultrathin sections of D05IB80. (d) olivine crystal in the FIB sections, (e-i) olivine, low-Ca pyroxene, high-Ca pyroxene, amorphous silica, and pyrrhotite in ultrathin sections. An inset in each TEM image is a selected area electron diffraction (SAED) pattern of each phase.

Figure 3. Chemical compositions of phases in the UCAMM D05IB80. (a) [Si + Al]-Mg-Fe

ternary diagram and (b) Si-S-Fe ternary diagram of GEMS grains. (c) Pyroxene quadrilateral showing chemical compositions of low- and high-Ca pyroxenes and Forsterite (Fo) mol.% histogram of olivine. (d) S-Fe-Ni ternary diagram of pyrrhotite. (e) FeO vs MnO and (f) FeO vs Cr_2O_3 diagrams of olivine and low-Ca pyroxene.

Figure 4. BSE image after SIMS analysis and $^{12}C^{14}N^-$, $^{16}O^-$ and $^{32}S^-$ isotopographs of UCAMM D05IB80.

Figure 5. (a) Back-scattered electron image, (b) optical image by a transmitted light, and (c) that by a reflected light of the surface of the polished cross-section of the UCAMM D05IB80. Tungsten deposition shown in (a) is the position where the focused ion beam (FIB) section was lifted out. (c) Transmitted optical image of the FIB section of the UCAMM D05IB80. The dark brown and the light brown area are contacted with a sinuous boundary. (d) High-angle annular dark-field scanning transmission electron microscopy (HAADF-STEM) image of the FIB section of D05IB80, where parallel grooves running from upper right to lower left are tracks formed by Cs^+ ion implantation during the SIMS mapping analysis. The two morphologies (smooth and globular) are indicated by arrows. Two box areas indicate

where elemental maps and high-resolution observation were performed (Fig. 9). Two GEMS grains and a polycrystalline olivine are also indicated.

Figure 6. Raman spectrum of the organic material in the UCAMM D05IB80. Background was subtracted. Peak position and full width at the half maximum (FWHM) of D_1 and G bands are shown as ω_{D1}, Γ_{D1}, ω_G, and Γ_G, respectively. In this spectrum, D_1 (red line), D_2 (green line), and G (blue line) bands were used to fit the spectrum. The residual graph is a difference between the raw spectrum and fitted spectrum.

Figure 7. (a) Carbon- and (b) nitrogen- distribution maps of the UCAMM D05IB80 obtained by STXM, and (c) carbon- and (d) nitrogen-XANES spectra of the regions 1, 2, and epoxy indicated in (b). Peak assignments are based on Leinweber et al. (2007) and Cody et al. (2008); peak A: 1s-π* transition for aromatic carbon (C=C*) at 285.1 eV, peak B: 1s-π* transition for N-heterocycles (C-N*=C), nitrile (C≡N*) or vinyl-keto carbon (C=C-C*=O) at ~286.6 eV, peak C: 1s-3p/s* transition for aliphatic carbon at CHx-C at ~287.5 eV, peak D: 1s-π* transition for carbonyl carbon in amide (NHx(C*=O)C) at ~288.0-288.2 eV and/or 1s-π* transition for carbonyl carbon in carboxyl or ester (OR(C*=O)C) at ~288.4-288.7 eV,

peak E: 1s-π* transition for imine (C=N*) at 398.8 eV, peak F: 1s-π* transition for N-heterocycles (C-N*=C) and/or nitrile (C≡N*) and/or at ~399.7 eV, and peak G: 1s-π* transition for amide (N*Hx(C=O)C) or 1s-3p/s* transition for amino (C-N*Hx) at 401.5 eV.

Figure 8. (a) BF TEM images obtained by in-situ observation of organic nanoglobules in the UCAMM D05IB80. (b) Moderate- and (c) high-resolution BF TEM images of the globular boundaries. (d) Moderate- and (e) high-resolution BF TEM images of the smooth boundary. Thin (< 2 nm) less-electron transparent layers indicated by arrows exist on the both kinds of boundaries shown in (c) and (e). (f) High-resolution TEM image of the thin layer in the globular boundary shows nanocrystals indicating 0.24- and 0.28- nm lattice fringes. (g) High-resolution TEM image of the thin layer in the smooth region shows there are no nanocrystals in the boundary.

Figure 9. (a) Elemental distribution maps of the smooth boundary shown as “Map 1” in Fig. 5e. The area near the boundary is enriched in C, O, Na, Si, S, K, and Fe. (b) Elemental distribution maps of the globular boundary shown as “Map 2” in Fig. 5e. The area near the boundary is enriched in C, O, Si, S, and Fe. The less electron transparent material is enriched

in O, Si, S, and Fe. A GEMS grain appears as an O, Mg, and Si enriched area in the lower right corner. (c) High resolution TEM image of a polycrystalline aggregate of tiny crystals included in a globule. The tiny crystals show 0.46- and 0.24- nm lattice fringes.

Figure 10. (a) The $^{12}C^{14}N^-$ and δD isotopographs before preparing a FIB thin section. Scale bars are 10 μm. Color bars are secondary ion counts for $^{12}C^{14}N^-$ isotopograph and isotope ratio with delta-value for δD isotopograph. (b) BSE image, $^{12}C^{14}N^-$, $\delta^{13}C$ and $\delta^{15}N$ isotopographs after making FIB thin section. Scale bars are 10 μm. Color bars are secondary ion counts for $^{12}C^{14}N^-$ isotopograph and isotope ratio with delta-value for $\delta^{13}C$ and $\delta^{15}N$ isotopograph.

Figure. 11. N/C versus O/C ratios of organics in the UCAMM D05IB80 (●, this study), the comet Wild 2 dust particles (□, Cody et al. 2008), the anhydrous IDP L20211R11 (■, Cody et al. 2008), types 1 and 2 chondritic insoluble organic solids (■, Alexander et al. 2007), and the UV irradiation products from interstellar analogues (○, Nuevo et al. 2011) (UV1 $H_2O:CH_3OH:CO:NH_3 = 100:50:1:1$, UV2 $H_2O:CH_3OH:CO:NH_3:C_3H_8 = 100:50:1:1:10$). The ratios were estimated from fitting of C-, N-, and O-XANES spectra.

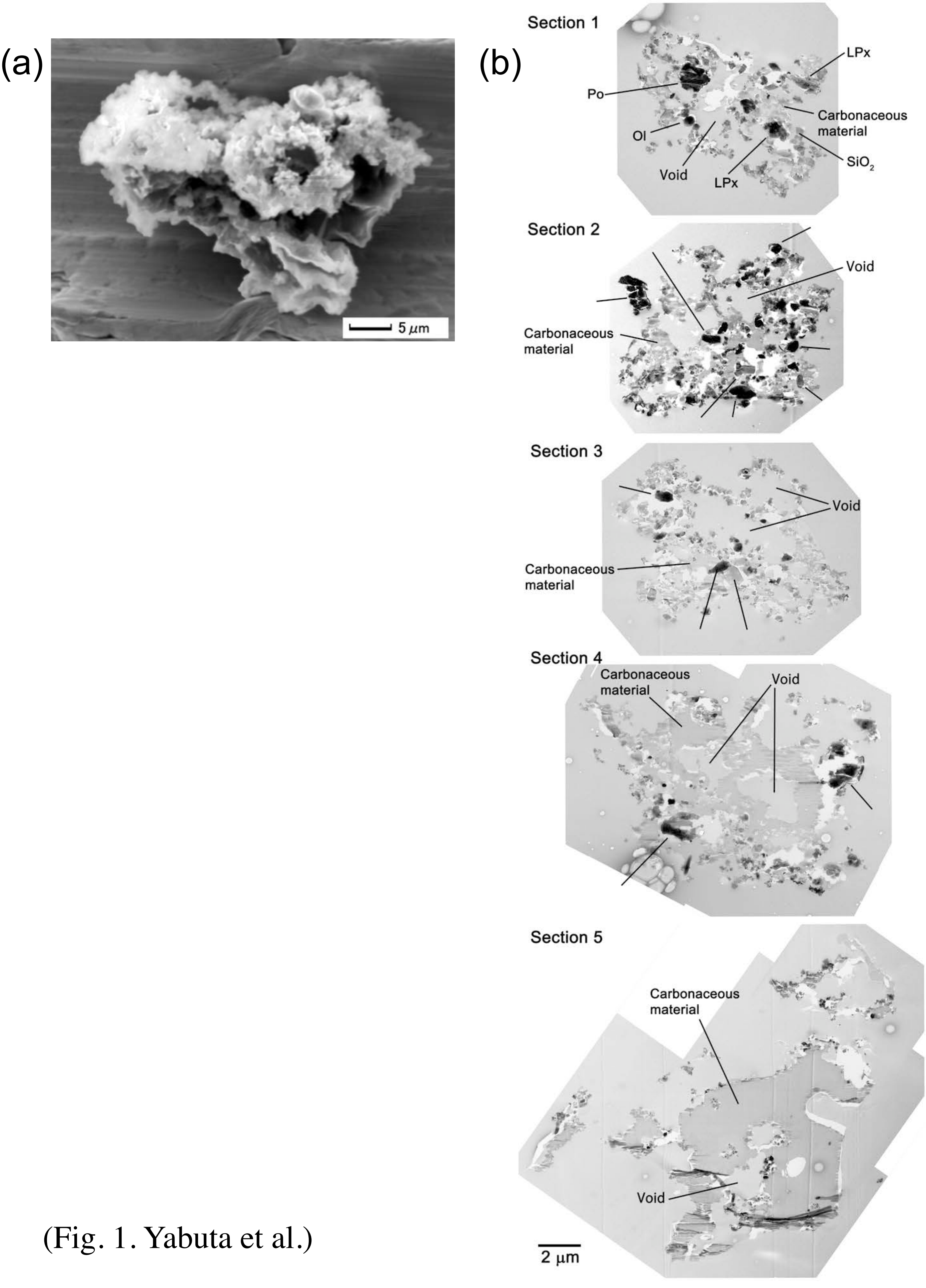

(Fig. 1. Yabuta et al.)

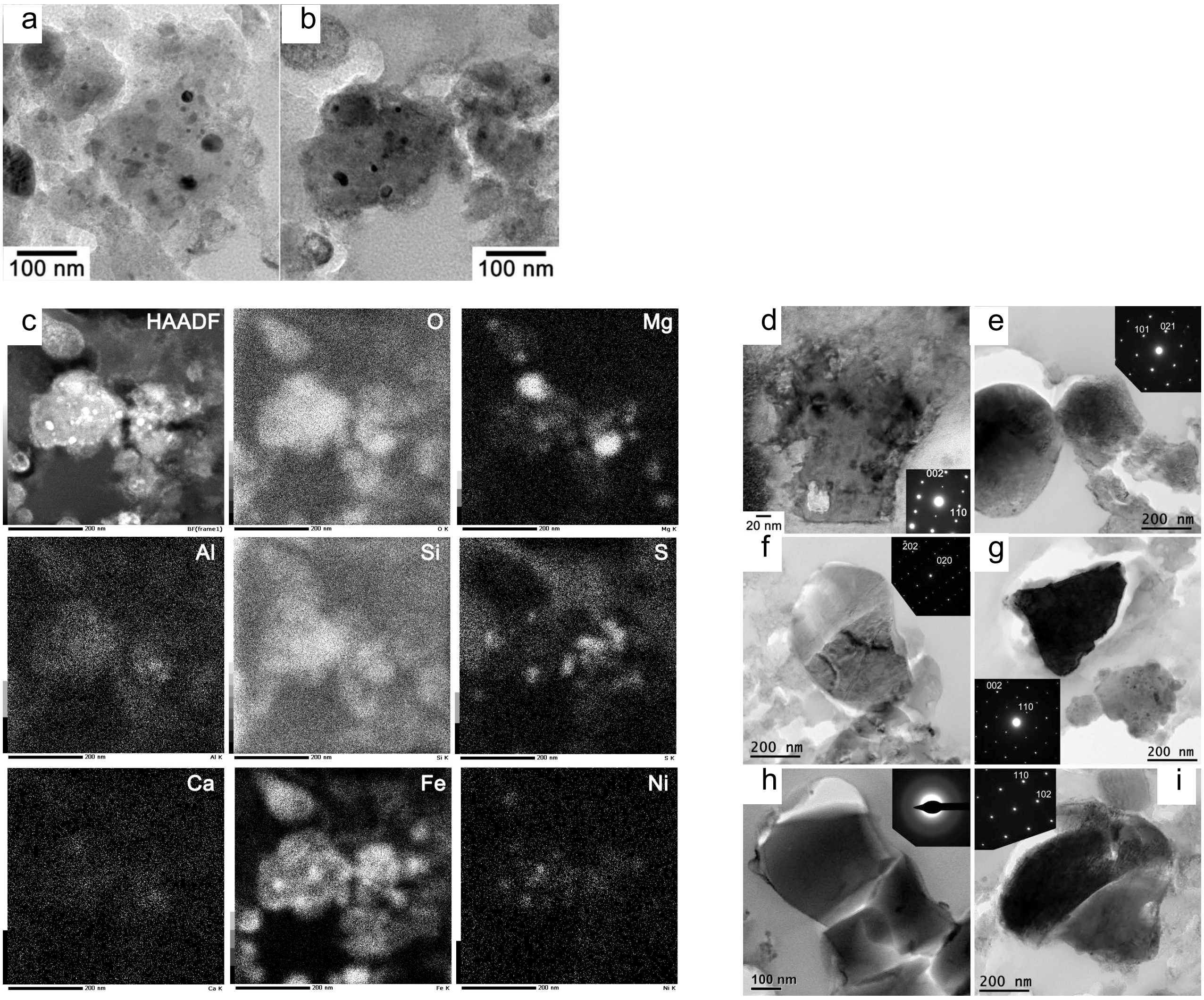

(Fig. 2. Yabuta et al.)

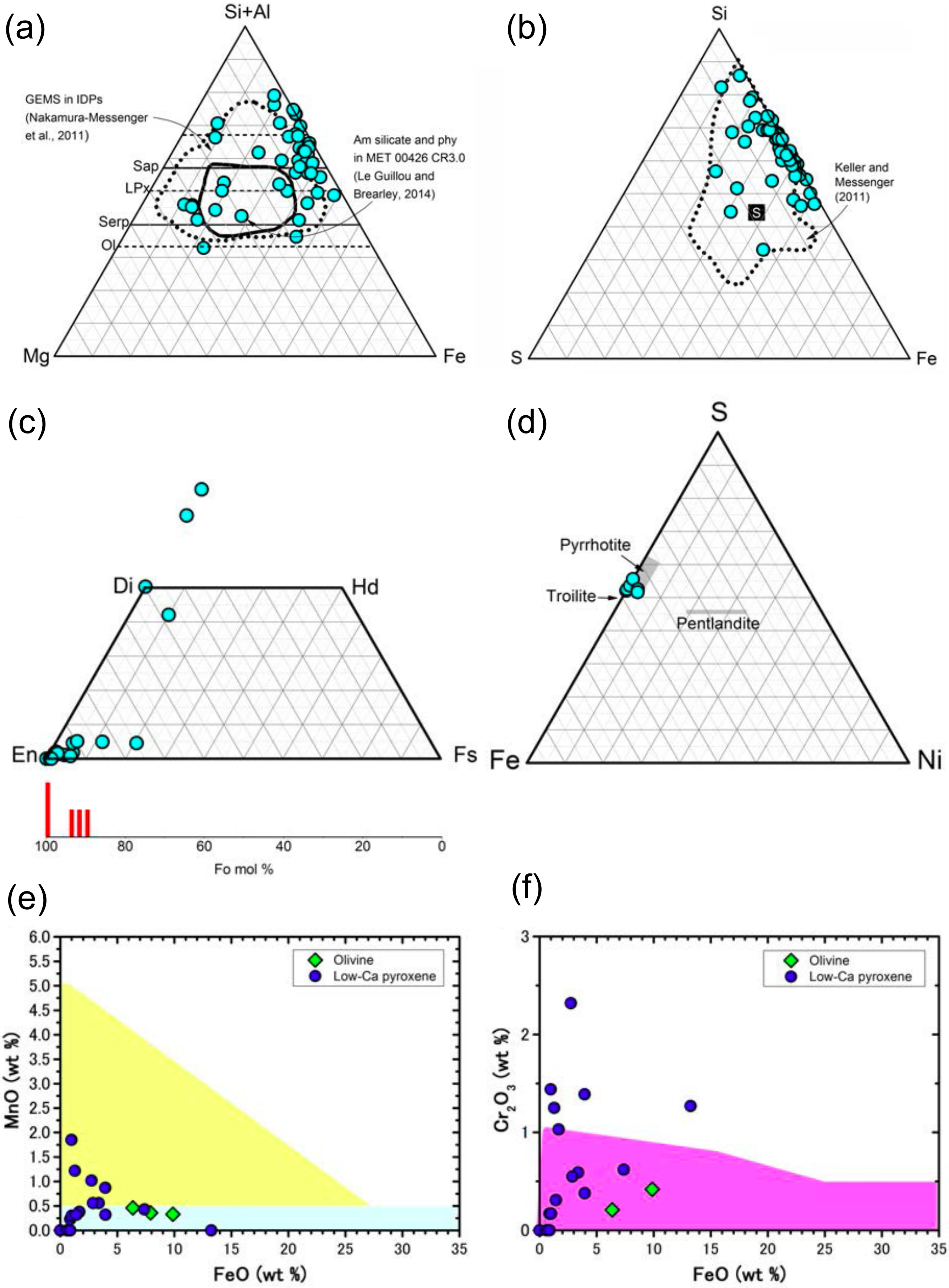

(Fig. 3. Yabuta et al.)

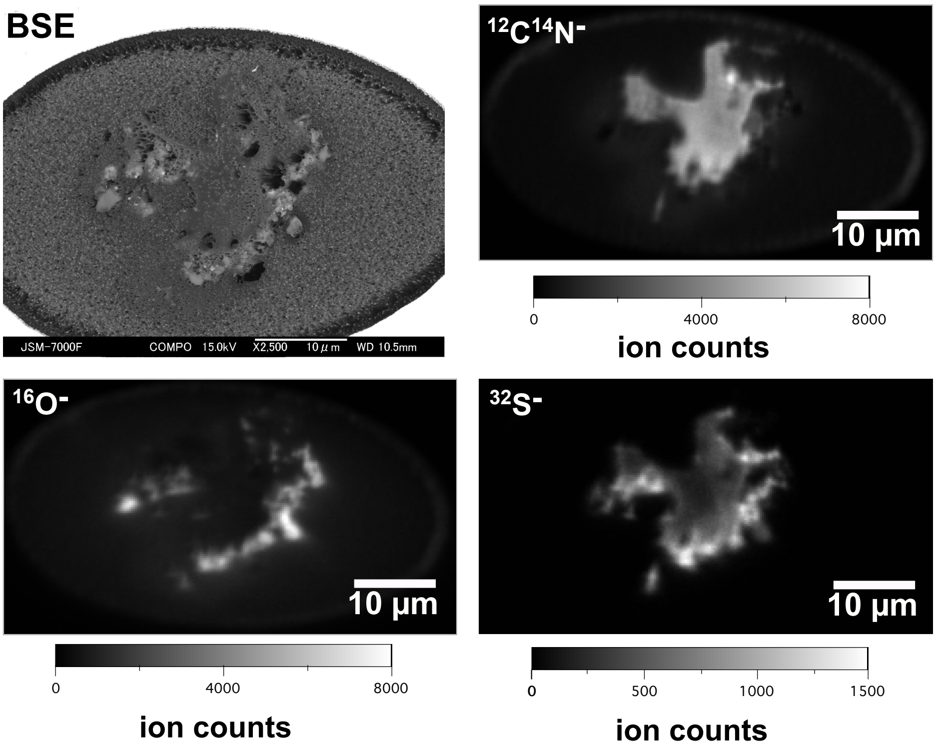

(Fig. 4. Yabuta et al.)

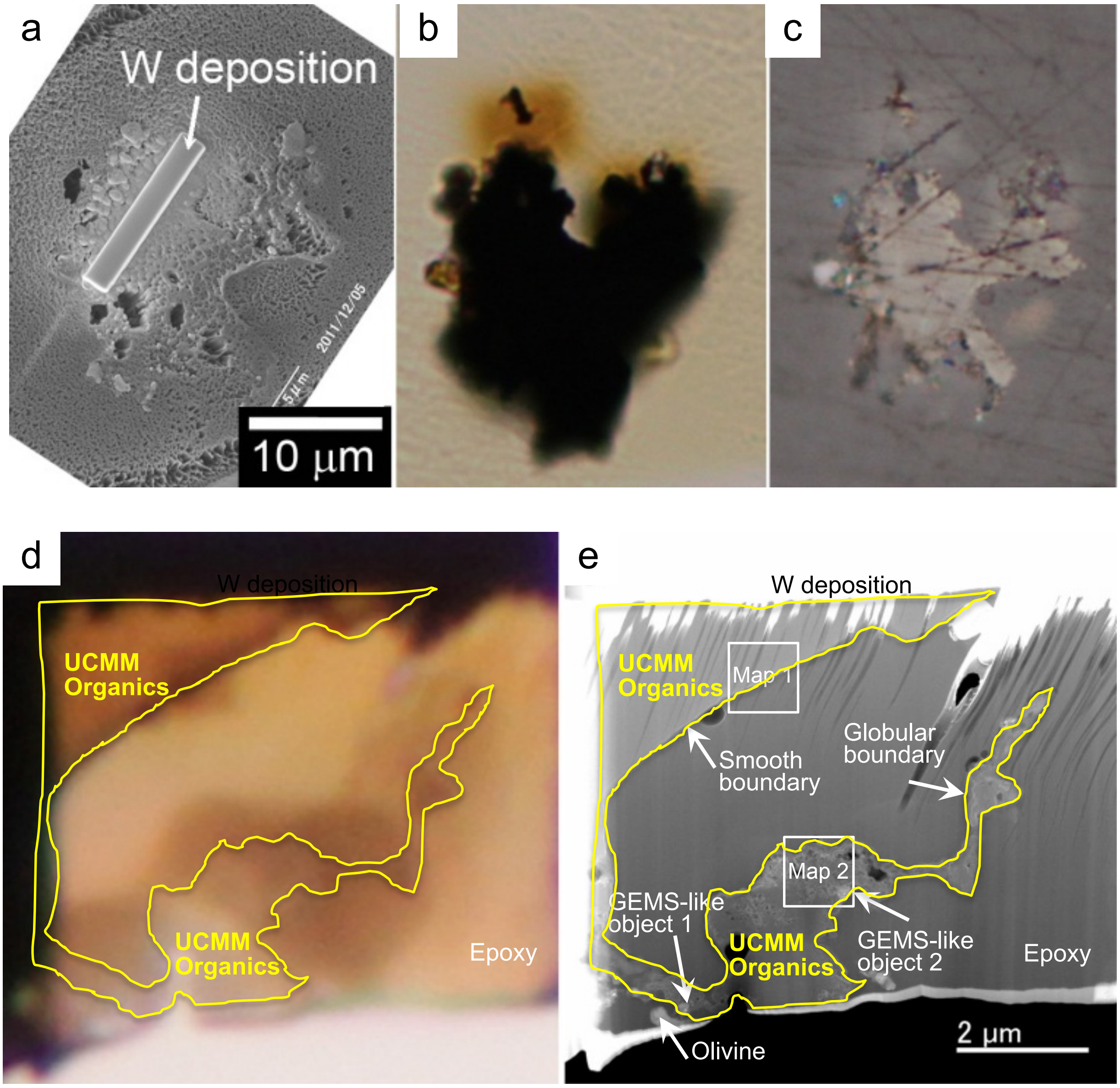

(Fig. 5. Yabuta et al.)

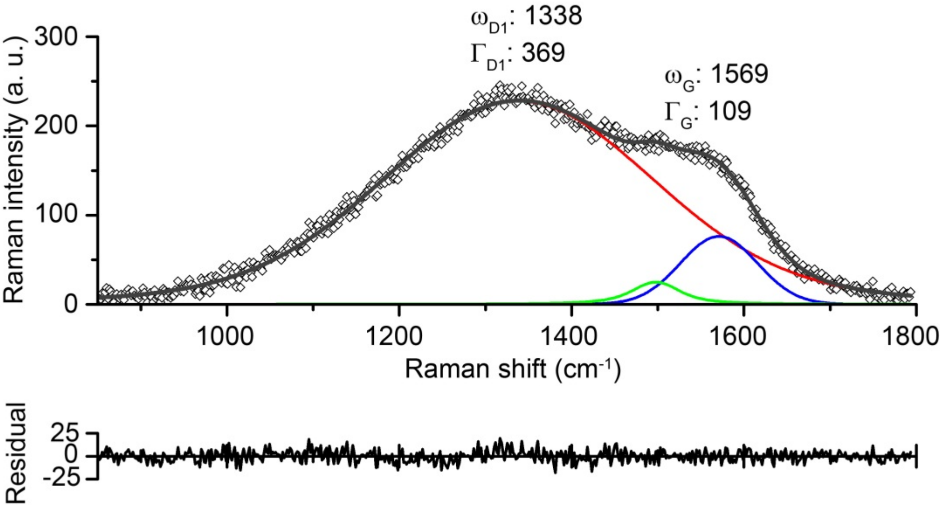

(Fig. 6. Yabuta et al.)

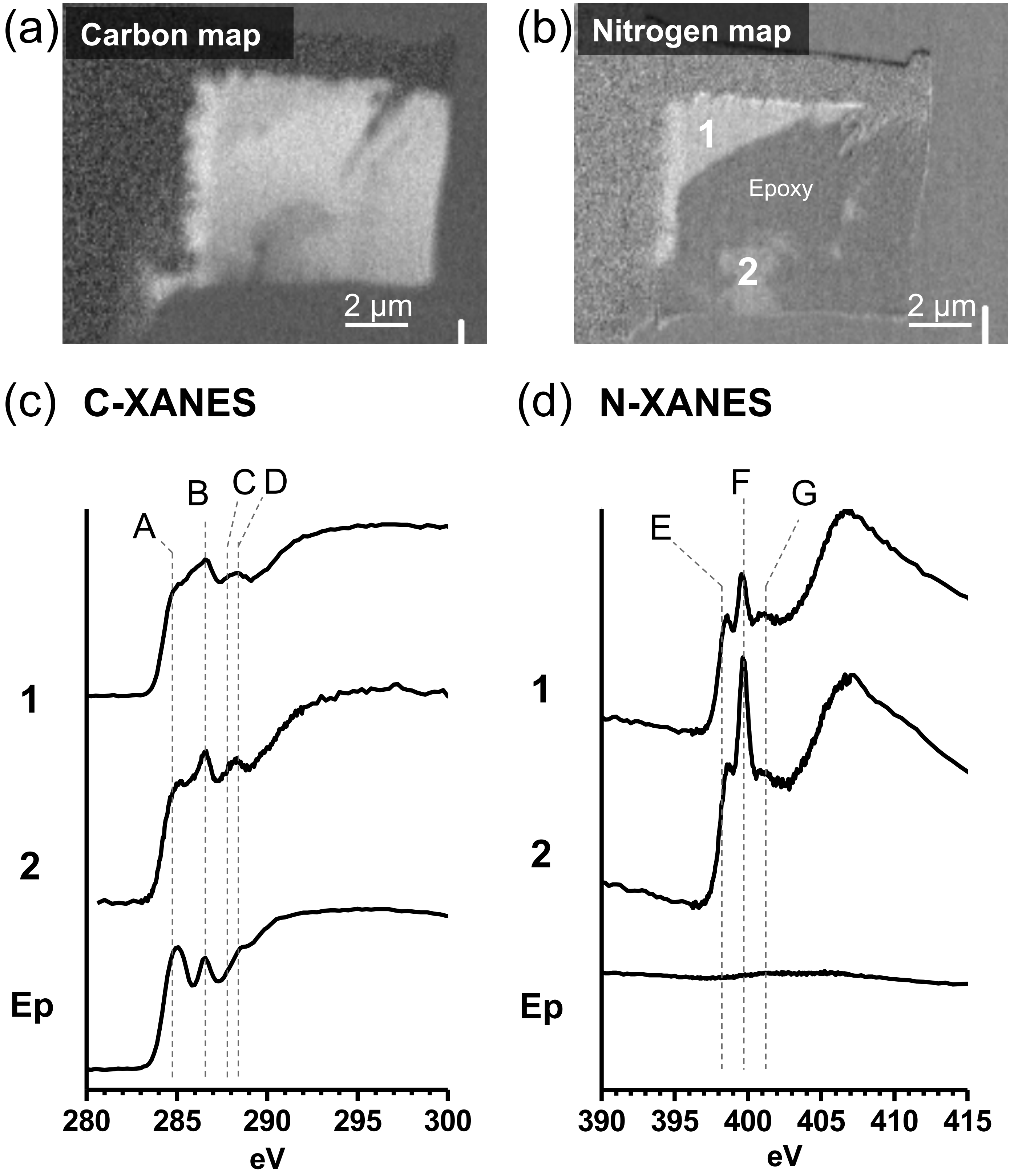

(Fig. 7. Yabuta et al.)

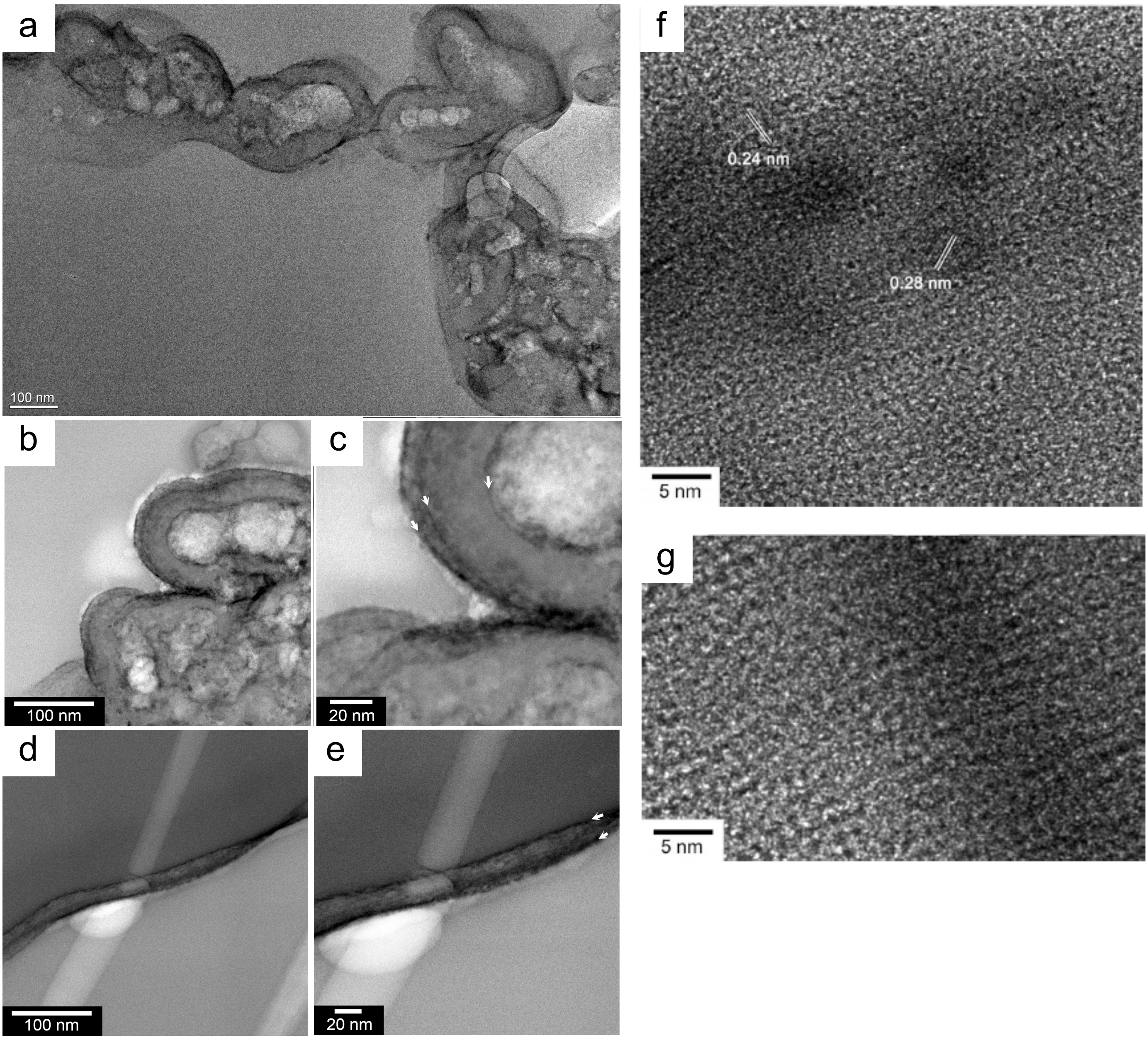

(Fig. 8. Yabuta et al.)

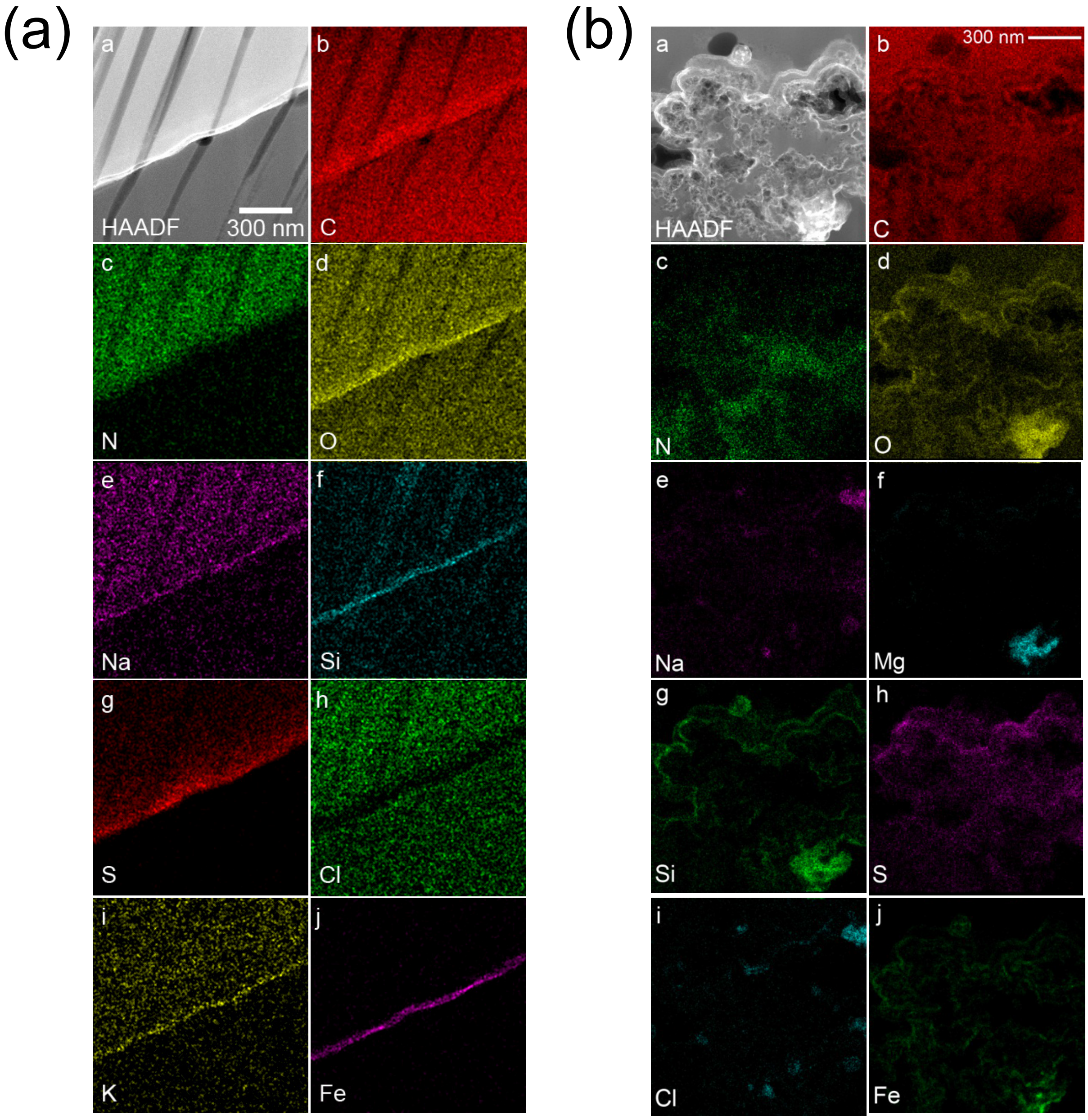

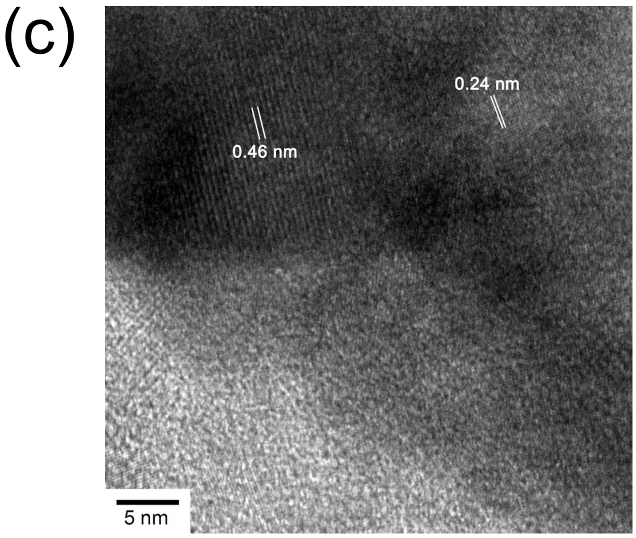

(Fig. 9. Yabuta et al.)

(a) Before FIB

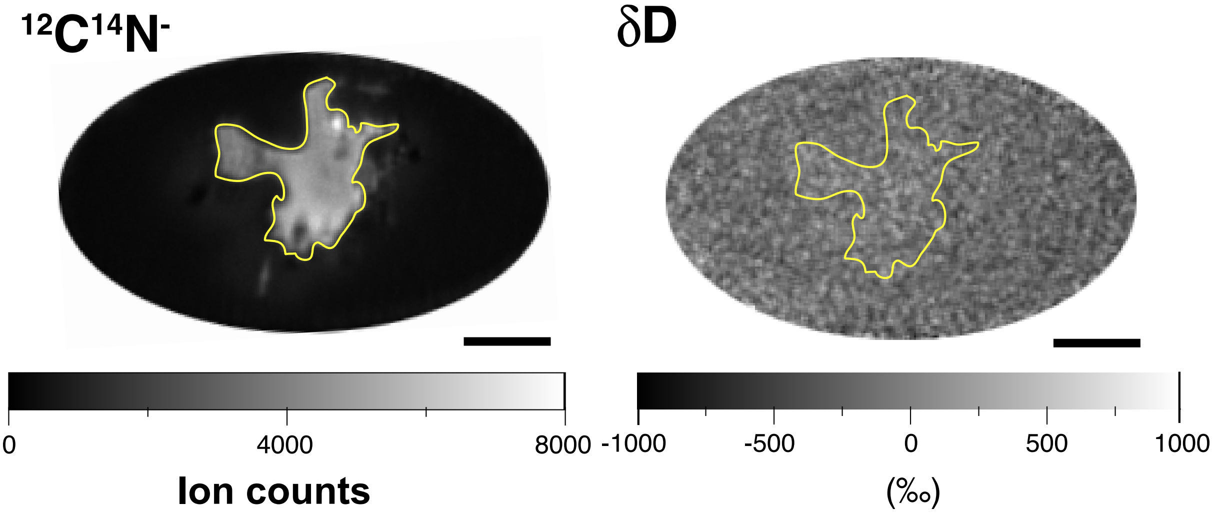

(b) After FIB

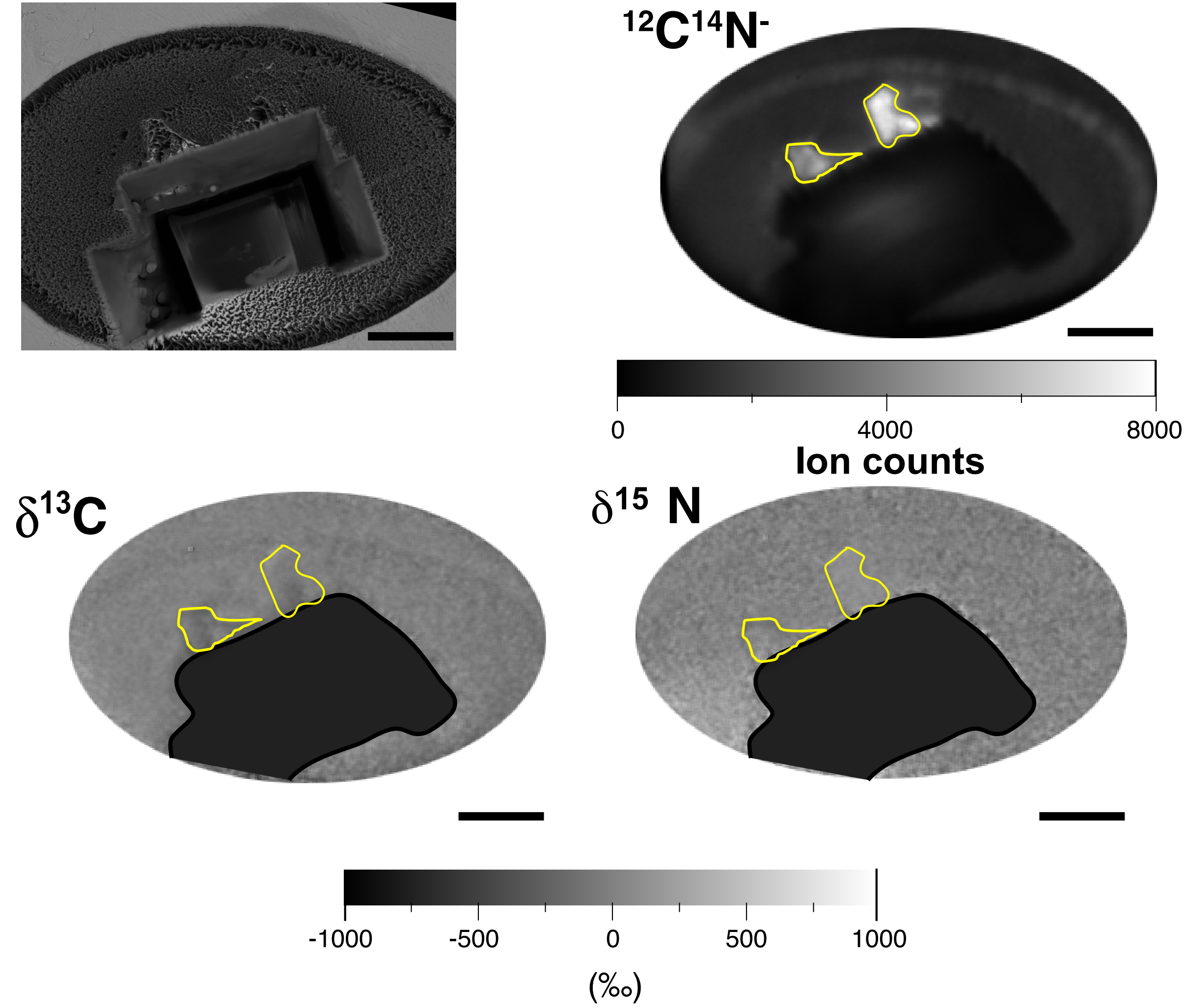

(Fig. 10. Yabuta et al.)

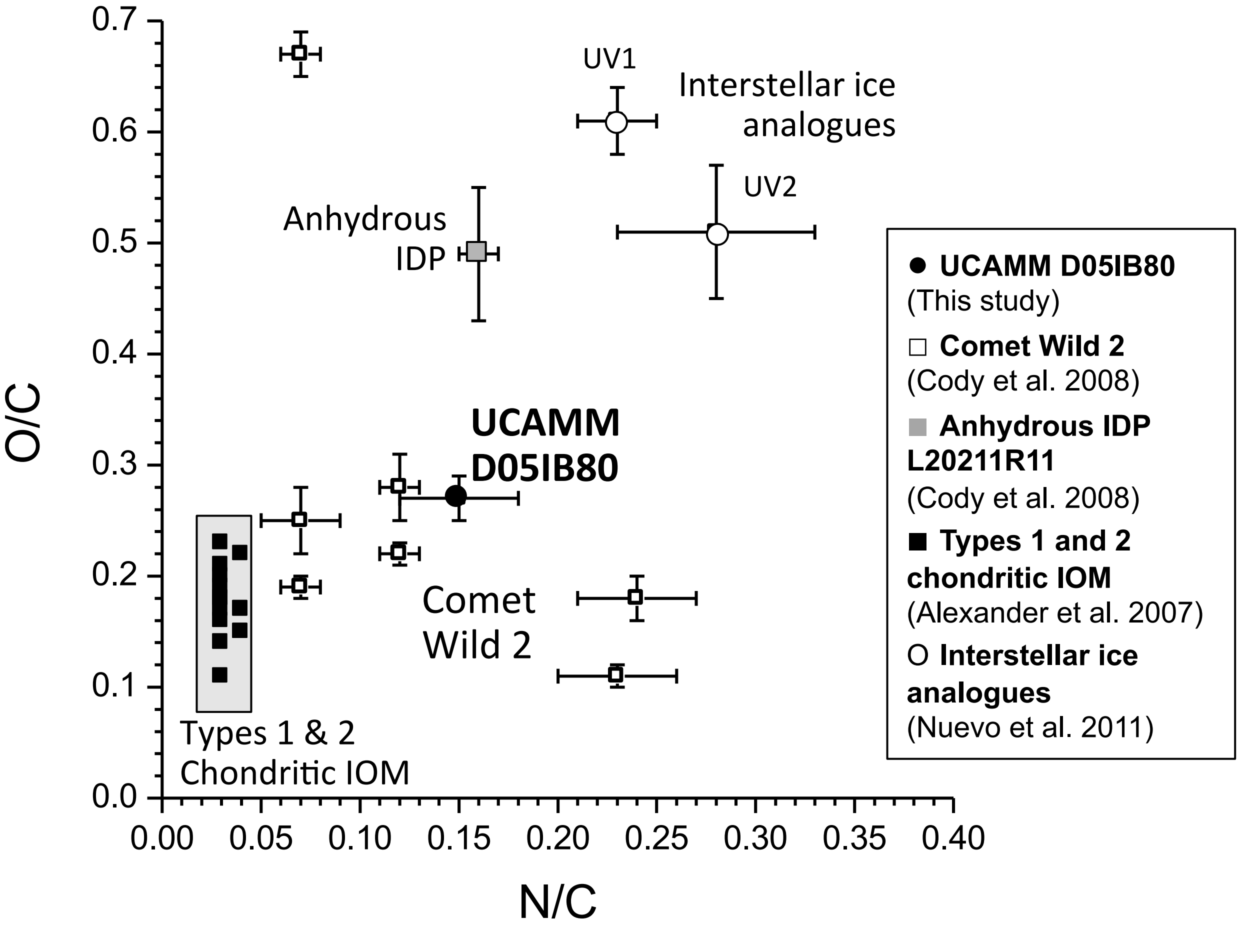

(Fig. 11. Yabuta et al.)